UNIVERSITY OF OKLAHOMA

GRADUATE COLLEGE

MODULATION OF RAINFALL BY THE SOUTH AMERICAN ALTIPLANO LAKES

A THESIS

SUBMITTED TO THE GRADUATE FACULTY

In partial fulfillment of the requirements for the

degree of

MASTER OF SCIENCE

by

JOSE MANUEL GALVEZ

Norman, Oklahoma

2005

MODULATION OF RAINFALL
BY THE SOUTH AMERICAN ALTIPLANO LAKES

A THESIS APPROVED FOR THE
SCHOOL OF METEOROLOGY

BY

[redacted]

Alan Shapiro

[redacted]

Michael Douglas

[redacted]

Evgeni Fedorovich

[redacted]

Lance Leslie

ACKNOWLEDGEMENTS

There are a large number of people that made this work possible. Firstly, I would like to thank Michael W. Douglas, my graduate research advisor, for providing the unique opportunity to pursue a Master's degree in meteorology at the University of Oklahoma. I very much appreciate his trust, encouragement, guidance and advice for my professional career. Special thanks also goes to Rosario Douglas, who, along with Mike have offered me continuous support, advice and friendship. I would also like to acknowledge the members of my committee - Evgeni Fedorovich, Alan Shapiro and Lance Leslie, for their insight and guidance during the completion of this work.

Thanks to the countless people in South America and the institutions that made this study possible: Carmen Reyes, Raquel Orozco, Teresa Garcia, Jonathan Cardenas, Roberto Catacora, Rimort Chavez and others, who worked thoroughly during the establishment of the raingauge network and collection campaigns; thanks to the volunteer observers for the altiplano activities; thanks to the Peruvian Weather Service (SENAMHI), the Instituto Geofísico del Perú (IGP), the Universidad Mayor the San Andres (UMSA), the Administración de Aeropuertos y Servicios Auxiliares para la Navegación Aérea (AASANA) and the Bolivian Weather Service (SENAMHI-Bolivia); many thanks to the NOAA Office of Global Programs (OGP) for funding this project.

My gratitude also extends to several others who were there for me along this path, including my office mates and friends John Freddy Mejia, Javier Murillo and Raquel Orozco, I have learned a lot from Freddy, not only as a person but academically, plus he has always been available for help and/or for motivation, especially during the hardest moments. Javier has always inspired security and trust, and I see in him an example to follow. He has also been available for advice whenever I needed it. Thanks to Raquel for her friendship, encouragement, and the countless moments of laughter. I think that our common origin, parallel careers, and the experience of coming to Oklahoma to pursue our degrees at almost the same time has created a special bond between us. Thanks to my dearest friends Hamish and Alex, your friendship has left a deep positive mark in my life during these years. I feel I wouldn't have been able to do this without your unconditional love, support, constant encouragement and advice. My gratitude to Pablo Lagos and the IGP team, who played an essential role on my education during the previous years to my arrival in the United States. Thanks to Celia Jones for her friendship, advice and valuable help with the paperwork, as well as to the many other friends that I have not mentioned.

Finally, I'm grateful to my family and friends back home for their unconditional love and support, and for their constant encouragement to try to follow my path and make my goals come true. This would not have been possible without you. I'd like to dedicate this work particularly to my little one, Jose Daniel, who has become my main motivation for personal growth.

TABLE OF CONTENTS

LIST OF TABLES

LIST OF ILLUSTRATIONS

ABSTRACT

Rainfall over the South American altiplano is modulated via mesoscale circulations induced by diverse land-surface contrasts present over the region. Nocturnal convective storms observed over Lake Titicaca represent 55% of the source of water for the lake. Above-normal lake levels can produce local and remote flooding, sometimes inundating areas as far south as the Salar de Uyuni, the largest dry salt flat in the world. This study focuses on describing the mesoscale circulations and rainfall induced by Lake Titicaca and Salar de Uyuni using observations collected during the South American Low Level Jet Experiment (SALLJEX 2002-3) and simulations carried out using the Weather Research and Forecasting (WRF) model. The study uses seven months of daily rainfall observations, three months of half-hourly infrared satellite data, 12 days of hourly wind profiles from pilot balloons and 3 months of NCEP Global Tropospheric Analyses.

Observations show that the nocturnal convective storms, only present over the lake, produce rainfall rates that almost duplicate the ones measured over the surrounding terrain. The lake- and salar-induced mesoscale circulations produce low-level divergence over both features during the day but late-night/early-morning convergence only over the lake. The period of largest convergence, in phase with the period of maximum frequency of nocturnal convection over the lake according to satellite data, seems to be associated with strong winds that develop over the eastern (western) slopes of the Andes and arrive at the lake (salar) by late afternoon. Composite analyses using satellite data and NCEP analyses indicated that mid-tropospheric above-normal mixing ratios over and east of the altiplano, consistent with above-normal convective activity over the region, were characteristic of the days in which the storms developed. Flow anomalies from the southeast suggest that the moisture source during these events may be located east of the southern Altiplano instead of east from the Lake Titicaca region. Consistent results found with the WRF model suggest that when the mid-tropospheric flow over the Lake Titicaca region is northeasterly, channeling of the flow near gaps in the mountain range to the east produces larger wind speeds over the lake compared to those found when the flow is southeasterly. Strong winds perpendicular to the lake axis seem to maintain the region of

low level convergence away from the lake, which suppresses the formation and maintenance of the nocturnal convection.

This study concludes that low-level convergence and moisture play an essential role in the development of the storms, but a moist and weak-wind environment near and over the altiplano boundary layer appears to be necessary for their development and maintenance. These factors, periodically present over the lake region during the rainy season, do not occur over the salar. Changes in the salar surface properties coupled with changes in the large-scale circulation pattern may be necessary for nocturnal convective storms to develop over the salar.

1. INTRODUCTION

1.1. Overview of this study

The South American Altiplano (herafter, altiplano) is an elevated plateau and closed basin located in the Central Andes between 14°S and 22°S. The landscape is characterized by a flat corridor that slopes gently from 3850 meters above sea level (mASL) at 15°S to 3650 mASL at 21°S. Mountain ranges with altitudes that exceed 6000 mASL surround the altiplano, and numerous lakes and dry salt flats (hereafter, salars) are found within it. Lake Titicaca and Salar de Uyuni are the largest lake and salar, with areas comparable to that of the island of Jamaica (~ 9000 km^2). Lake Titicaca, at 3810 mASL, is located in the highest and northernmost sector of the basin, whereas the Salar de Uyuni, at 3653 mASL, lies at the lowest and southernmost part (Figures 1 and 2).

Paleoclimate studies focused on the altiplano have revealed that transitions between salars and shallow lakes have occurred several times in the past with different intensities (Kessler, 1984; Blodget et al., 1997; Baker et al., 2001; Sylvestre et al. 2001; Trauth et al. 2003; Placzek et al. 2004). High-resolution climate records, found in the form of sediments accumulated in altiplano lakes and glaciers, have motivated numerous paleoclimate studies which have revealed that the region was exposed to dry and wet periods in the past, a number of them with durations of several millennia. Some of these periods lead to the development of different transient paleolakes. The maximum paleolake expansion occurred between 15000 and 13000 B.P. leading to paleolakes Tauca and Titicaca (Figure 3). Published radiocarbon dates indicate that paleolake Tauca existed from about 18000 to 13000 B.P., and attained a maximum depth of 140 m (Baker et al. 2001). Variations of the planetary circulation and insolation over the altiplano appear to be the main driver of these cycles. Baker et al. (2001) mentioned that the main wet and dry phases on the Altiplano occurred, respectively, in phase with summertime (January) insolation maxima and minima. Abbott et al. (2003) suggested that over millennial timescales changes in insolation should influence the location and strength of the Bolivian High and strongly affect the precipitation regime of the region. On the other hand, periods of colder temperatures in the eastern north Atlantic with respect to the western north Atlantic, which correlate with enhanced northeast trades, lead to increased advection of moisture to the Amazon and the altiplano (Baker et al. 2001).

Although different authors have explored the role of the planetary circulation on changes in the altiplano rainfall, the role of mesoscale processes, especially those induced by the lakes and salars, has apparently not yet been considered with detail in the literature.

The above described salar-lake fluctuations have been observed over smaller timescales during recent history. Prolonged rainy conditions in the upper altiplano cause the lake levels to rise and overflow, which produces (1) flooding in the populated Lake Titicaca sector (Bourges et al, 1992) and (2) a southward migration of the overflowing waters, which sometimes fill the Salar de Uyuni with several centimeters of water (Sylvestre et al. 2001).

Most of the precipitation falling over Lake Titicaca appears to be produced by nocturnal convective storms that appear to be related to the land-lake temperature contrasts that drive lake breeze circulations. Nocturnal convection is however not observed over the generally dry Salar de Uyuni. If the development of nocturnal convection were mainly a function of the strength of the convergence over a lake, a salar flooded with a sufficiently deep layer of water should trigger the nocturnal convection mechanism by modifying the strength of the nighttime land breezes and by changing the low-level stability. Persistent convection over the salar would preserve and enlarge the depth of the water layer eventually turning the salar into a lake and possibly shifting the overall altiplano climate towards wetter conditions.

The importance of the above hypothesis, which is very speculative, is that it involves mesoscale meteorological processes in the change from a dry climatic state to a wet one over the altiplano. Such a mesoscale-induced climatic state transition, if it exists, would be very difficult to incorporate into climate models attempting to model paleoclimate states of the altiplano, since their spatial resolution is far too coarse to model the mesoscale processes producing the rainfall associated with the altiplano lakes.

One means to begin to evaluate the above mentioned hypothesis is to measure the strength of the circulations induced by the lake and the salar, which is the focus of the present study. Describing how Lake Titicaca and the Salar de Uyuni modulate rainfall through induced mesoscale circulations will provide (1) a background to start understanding the role of the mesoscale processes on the salar-lake transitions and (2) describe the atmospheric conditions that lead to large rainfall rates for regional weather and climate forecasting improvements.

This study uses special field measurements made over the altiplano during 2002-3 to describe the characteristics of mesoscale circulations associated with large lakes and salars. It then demonstrates that certain aspects of these circulations can be reproduced with a high resolution weather prediction model.

1.2. Region of study: the South American altiplano

1.2.1. General geography of the altiplano

The altiplano is an elevated plateau (~ 3700 mASL) located in the central Andes between 14°S and 22°S (Figures 1 and 2). It is also a closed basin that extends over 198,000 km^2 (Blodget et al., 1997) from southern Peru into southern Bolivia and northern Chile. The basin is bounded by the Amazon and the La Plata basins to the east and the Atacama Desert to the west. Most of the landscape consists of a 250 km-wide plane corridor that slopes from 3850 mASL in the northern end to 3660 mASL in the south. Small mountain ranges and hills interrupt sectors of the corridor, and large mountain ranges with peaks that exceed 6000 mASL surround the basin. The highest point, on the western side of the altiplano, is the Sajama volcano in western Bolivia with an elevation of 6520 mASL.

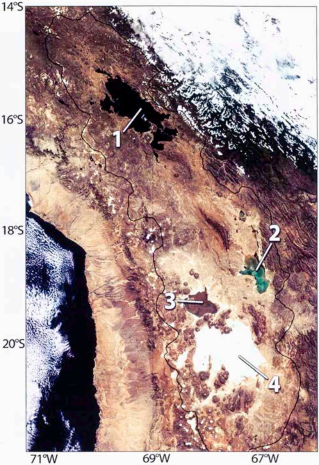

Figure 1. MODIS image of the Altiplano. The figure shows the current lakes and dry salt flats: Lake Titicaca (1), Lake Poopo (2), Salar de Coipasa (3) and Salar de Uyuni (4). The edge of the Altiplano basin is indicated with a thin and continuous black line (7). Brown waters over Salar de Coipasa indicate the presence of water covering the salty surface, which suggests that the image was taken during a wet period.

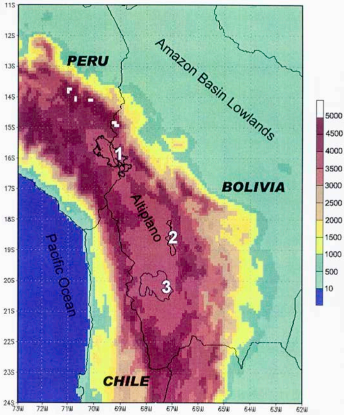

Figure 2. Ten kilometer resolution topography of the Altiplano region in mASL. Lake Titicaca (1), Lake Poopó (2) and Salar de Uyuni (3) are indicated. The country border are indicated with thin lines and the country names with bold italic fonts. Three distinctive geographical regions: the Amazon Basin lowlands, the Pacific Ocean and the altiplano are indicated with plain fonts.

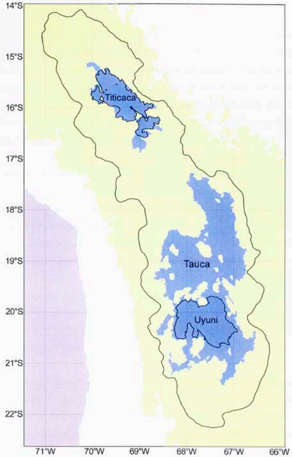

Figure 3. Map of the Altiplano showing the location of Lake Titicaca and Salar de Uyuni (solid black line), and paleolakes Tauca and Titicaca (light blue shading) during the maximum paleolake expansion. The terrain higher than 3000 mASL is shaded in light brown and the edge of the Altiplano basin is indicated with a solid black line. The image was reconstructed from Blodget et al (1997).

The basin's characteristic ecosystem is the puna, a formation of rigid gramineae grasses and dwarf bushes with coriaceous leaves and forests of queñoa (Polylepis) and other trees in sheltered regions (Jellison et. al. 2004). The rainfall gradient leads to steppes (Figure 4 and Figure 5) north of 17°S versus shrub lands and deserts south of this latitude. Barren or sparsely vegetated landscapes are common near the Chilean border and tundras shape the highest elevations (Figures 6 and 7). Glaciers can be found in sectors of the eastern and western mountain ranges, generally above 5500 mASL. The animals most characteristic of these ecosystems are condors and flamingoes, and various camelids, including llamas, alpacas, vicunas and guanacos (Jellison et. al. 2004).

Numerous lakes and salars describe the basin's hydrological system. From these the largest are Lake Titicaca, Lake Poopó, Salar de Coipasa and Salar de Uyuni. Lake Titicaca (Figures 5 and 6), the major focus of the present study, is the largest lake with a surface area of 8170-8400 km^2 and a volume of 932×10^6 m^3 (Schwerdtfeger, 1976; Constantini, 2003; Ronteltap, 2004). It is centered at 16°S and 69.5°W and at 3808 mASL in the upper basin located in the northern Altiplano. Its maximum length is 195 km, its average width is 50 km, and its maximum depth of about 300 m, which make it the highest navigable lake in the world. The Salar de Uyuni (Figure 11), is the largest salt flat in the world (Baker et al. 2001), is located in the southern end of the altiplano (centered at ~20°S) at an elevation of 3653 mASL, and has a surface area of about 10000 km^2 (Sylvestre et al. 2001).

The hydrological balance of Lake Titicaca, described by Ronteltap (2004), indicates that ~45% of the water input for Lake Titicaca is provided by rivers and stream flow whereas ~55% comes from precipitation. Diffuse groundwater leakage into the lakes from aquifers is believed to be negligible. Of the total water input, about 95% evaporates and 5% is transported away from the lake by the Rio Desaguadero. The discharge varies considerably in the course of the year, from practically zero during the dry season up to 10 times the average discharge in the rainy season (Ronteltap, 2004). When the latter situation occurs, generally during the wettest stages of the rainy season, the waters of the lake flow into Lake Poopó, then into the Salar de Coipasa and sometimes as far south as

Figure 4. Lake Titicaca landscape. Notice the grassy surface and the large size of the lake.

Figure 5. Group of pilot balloon observers established at Conima during the Lake Titicaca Field Experiment 2003. Notice the northern Altiplano landscape.

Figure 6. Volcano located in the southern Altiplano. Notice the sparse vegetation and snow capped top.

Figure 7. Observing site established near the center of the Salar de Uyuni during the Salar de Uyuni Field Experiment in 2002. Notice the highly reflective salar surface and dimensions of the salar.

Salar de Uyuni. A brine sometimes as deep as 25 cm develops over the salars in places, but evaporates during the dry season to expose the salty surface (Sylvestre et al. 2001).

Politically, the altiplano is shared by Bolivia, Peru and Chile. Lake Titicaca is divided in two by the Peruvian-Bolivian border, placing the westernmost side in Peruvian territory. The entire region is sparsely populated due to harsh climate conditions and scarce hydrological resources. The southern altiplano is the least populated with densities lower than 1 inhabitant per km^2 from the Salar de Uyuni southward. Most of the population is concentrated in the northern third of the altiplano, particularly near Lake Titicaca where the density ranges between 10 and 40 inhabitants per km^2 in response to more abundant resources. The lake itself provides water to nearly 3 million people (Revollo et al., 2003), including parts of the city of La Paz, Bolivia. The economical activities in the altiplano are based on agriculture, livestock and mining.

1.2.2. Overview of the altiplano climate

The climate of the altiplano is semi-arid with annual rainfall rates that range between ~200 mm yr^{-1} in the southwestern sectors to ~800 mm yr^{-1} in the northeast (Blodget et al., 1997; Abbott et al. 2003). Other authors have indicated that rainfall decreases southwards from 390 to 100 mm yr^{-1} in the southern Bolivian Altiplano (Sylvestre et al. 2001), and that the few climatic stations located near the tropic of Capricorn at an altitude of about 4000 mASL register less than 180 mm yr^{-1} (Vuille et al. 1997). The largest rainfall rates among the entire altiplano (larger than 800 mm $year^{-1}$) are observed in the vicinity of Lake Titicaca. Satellite imagery and local observations suggest that this region of high rainfall is partly explained by the contribution of nocturnal convective storms that generate over the lake mainly during the rainy season. Figure 8, reconstructed from an analysis presented by Schwerdtfeger (1976) displays mean annual rainfall accumulated between 1957 and 1961. The analysis shows a region of more than 1100 mm $year^{-1}$ over the lake contrasting with less than 800 mm $year^{-1}$ around it. The effects of the lake on rainfall can also be observed in Figure 9 which displays monthly rainfall for Puno and Juliaca, located at ~40 km apart. Between December and April the rainfall rates are larger

(10 – 40 mm month^{-1}) in Puno than Juliaca, which suggests a contribution from lake-induced convection since Puno is located on the lakeshore whereas Juliaca lies inland. This figure also shows lower rainfall rates in Oruro, located 2.5° south from Puno and Juliaca illustrating the north-south rainfall gradient.

The seasonal cycle of rainfall over the altiplano is quite pronounced with a defined rainy season that coincides with the austral summer (Figure 9). According to Garreaud and Aceituno (2000), more than 90% of the precipitation occurs between November and March, with January and February being the rainiest months. Baker et al. (2001) and Sylvestre et al. (2001) indicated that 50 to 80% of the total annual precipitation occurs between December and March. The rainy season is more prolonged in the northern portion of the Altiplano than in the south, in response to lengthier periods of large boundary layer moisture content. The summer precipitation is convective and occurs in the form of afternoon thunderstorms (Garreaud and Aceituno, 2000; Aceituno, 1997; Schwerdtfeger, 1976) that develop over land. The convection is associated with a deep layer of conditional instability during the summer afternoons and boundary layer mixing ratios exceeding ~ 7 g kg^{-1} (Garreaud 1999).

The major source of moisture for the altiplano is the tropical continental air that characterizes the Amazon basin located to the east. During the summer, an anticyclonic circulation, the Bolivian High, develops in the upper troposphere leading to periods of upper- and mid-tropospheric easterly flow over the altiplano. The position and strength of this system is intrinsically linked to precipitation anomalies over the Altiplano, featuring an intensification and southward displacement during wet episodes, while a weakening and northward displacement can be observed during dry periods (Aceituno and Montecinos 1993; Vuille et al, 1998; Lenters and Cook, 1999; Vuille, 1999; Abbott et al. 2003). These easterly flow events are the main drivers of convective events in the Altiplano. As Garreaud (2000) suggested, mid-tropospheric easterly flow accelerates the moisture flux through the eastern slopes of the Andes through downward momentum transport, leading to large boundary moisture contents, many times exceeding the above mentioned 7 g kg^{-1} threshold. On the other hand, mid-tropospheric westerly flow

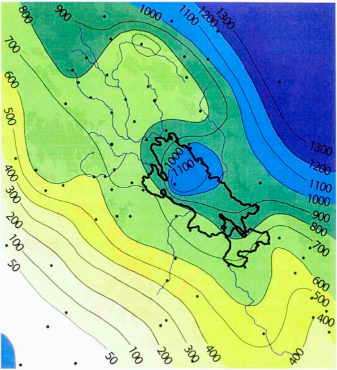

Figure 8. Mean Annual Rainfall in the Lake Titicaca (mm year^{-1}) area accumulated from 1957 to 1961. This figure was extracted from Schwerdtfeger (1976) after Kessler and Montheim (1968) and reformatted. Lake Titicaca is indicated with a thick black solid line, the elevations above 4500 mASL with a shading, the main rivers with blue lines, and the raingauges with black dots.

conditions, persistent during the winter and intermittent during the rainy season, advect dry air from over the Pacific Ocean basin leading to near surface moisture readings lower than 3 g kg^{-1}, which in turn suppress any type of moist convection. The high aridity that characterizes the region west of the Altiplano (i.e. the Atacama desert and southeastern Pacific Ocean), demonstrated by the lack of glaciers even on the highest volcanoes in northern Chile (Vuille et al 1997), is associated with widespread subsidence in this region associated with the south Pacific anticyclone.

Altiplano mean annual temperatures range from below freezing in the highest elevations to ~10°C in the vicinity of Lake Titicaca (Atlas de Bolivia, 1997). The diurnal temperature oscillations are remarkable, especially during the winter, as suggested by Figure 10. An extreme example is the temperature measured at Charaña, located in the central-western Altiplano at 4057 m ASL, during August 1969 when an average diurnal range of 31.9°C and a largest daily range of 42.5°C occurred (Schwerdtfeger, 1976). The largest diurnal cycles can be encountered in the south and west in response to drier conditions, and in higher elevations in response to larger amplitudes in the diurnal cycle of radiation. Furthermore, lakes modulate the temperature as seen in Figure 13, where the differences in the amplitude diurnal cycle at Puno and at Juliaca are on the order of 4°C during the rainy season and 10°C during the dry season. Lake Titicaca is sufficiently large and deep to conserve its surface temperature (annual mean is 13°C, Carmouze, 1991) throughout the year.

The seasonal cycle of temperature results from combination of a component form the diurnal cycle of solar radiation, the effects of latitude and the atmospheric moisture content. The variation of the maximum temperature (14-20°C during the rainy season 12-17°C during the dry season) is the less with larger moisture contents and cloudier skies during the warm season which contrasts with dry and cloudless conditions during the winter (Figure 13). Minimum temperatures exhibit a larger seasonal cycle, especially away from the lakes, and oscillate between 2 and 5°C during the rainy season versus –13 to –5°C during the dry season (Figure 10).

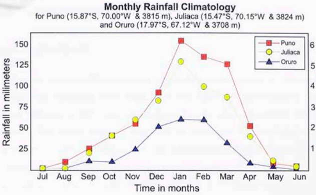

Figure 9. Monthly rainfall climatology for Puno, Juliaca and Oruro. The climatologies were prepared with data from 1964 to 1980 for Puno, 1960 to 1995 for Juliaca and 1960 to 1969 for Oruro. The first two datasets were acquired from Instituto Geofísico del Perú and the latter from Schwerdtfeger, 1976.

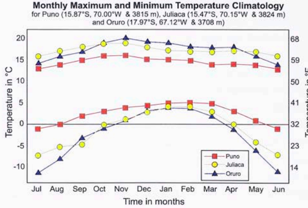

Figure 10. Monthly maximum and minimum temperature climatology for Puno, Juliaca and Oruro. The climatologies were prepared with data from 1960 to 1996 for Puno, 1961 to 1991 for Juliaca and 1960 to 1969 for Oruro. The first two sites were obtained from Instituto Geofísico del Perú (Geophysical Institute of Perú). Oruro was obtained from Schwerdtfeger, 1976.

1.3. Historical perspective for this study

1.3.1. PACS-SONET

The Pan American Climate Studies Sounding Network (Figure 11), or PACS-SONET (Douglas and Fernandez, 1997; Peña, 1999), is a research project funded by the Office of Global Programs (OGP) from the National Oceanic and Atmospheric Administration (NOAA). The project began in 1997 with the main goal being to better describe and explain the circulation variations above the intertropical Americas. Given the high cost of a radiosonde observation, the radiosonde networks operated routinely in the tropical Americas are sparse compared to those operated in developed countries. The PACS-SONET is based on an alternative solution to enhance the spatial and temporal resolution of these networks which is the operational use of pilot balloon stations, given that a pilot balloon observation represents a cost of ~10% that of a radiosonde observation.

The PACS-SONET began initially with 12 pilot balloon stations distributed from southern Mexico to Peru that were operated with the objectives of determining: (1) The circulation anomalies associated with wet and dry spells over Central America, (2) the amplitude of the diurnal cycle of winds over the region and how this may affect the assessment of the climatological mean flow, and (3) the extent of differences between observations and the NCEP reanalyses, with the aim of strengthening confidence in these analyses for studies of climate variability. Due to changing the extensions broadened coverage over Latin America and added new specific goals to the project. Two stations installed in Paraguay and six in Bolivia, initially supported with NASA funds to provide synoptic coverage for the Large-Scale Biosphere-Atmosphere (LBA) measurement centered in Amazonia. Two of these sites were established on the altiplano, at La Paz and at Uyuni on the edge of the Salar de Uyuni. Although these sites were established with the primary objective of explaining the variability of the low-level flow east of the Andes, they generated interest in the circulation over the South American altiplano.

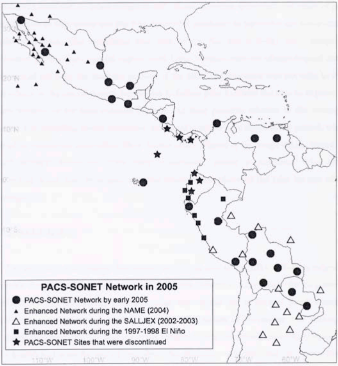

Figure 11. Sites operated by the PACS-SONET project. The solid circles correspond to the PACS-SONET operational sites by early 2005. The small solid triangles are the sites operated during the NAME in 2004. The large white triangles are the sites operated during the SALLJEX in late 2002 and early 2003. The squares are the sites operated during the 1997-1998 strong El Niño. The stars are stations operated by PACS-SONET in the past.

As part of the PACS-SONET activities, a 3-week workshop and short field experiment were carried out in Bolivia during December 2000. The main goal was to spin up the meteorological activities in this country to support the pilot balloon network that had been established in 1999. The second objective was to make South American individuals involved on meteorological and related activities appreciate the value of pilot balloon data so they could use the PACS-SONET database, in particular the observations made in Bolivia. The workshop was held in La Paz and a 3-day field campaign, motivated by the high rainfall region over Lake Titicaca seen on climatological maps, was carried out over the southern portion of the lake. The objective was not only to train individuals in the use of optical theodolites to follow pilot balloons but also to explore the characteristics of the lake-induced breezes and their possible relation to the nocturnal storms. The sampling period coincided with a quite active lake effect storm period, which served as additional motivation for a further study. Figure 6, an image taken during the PACS-SONET December 2000 field experiment, shows a nocturnal lake effect convective storm that developed near the southwestern shore of the lake on one of the evenings.

1.3.2. SALLJEX

The Bolivian observations that started in 2000 as part of the LBA activities helped to motivate the design ad development of the South American Low Level Jet Experiment (SALLJEX). The SALLJEX field campaign was carried out in central South America during the rainy season of 2002-3 starting in the month of November and ending in February. Enhanced surface and upper air meteorological observing networks (Figure 13) were established with the aim of describing the structure, variability and role of the South American Low Level Jet (i.e. SALLJ, a low-tropospheric northwesterly air current found east of the central Andes) on the moisture transport from the Amazon basin into the Plata basin. Three SALLJEX projects were organized by the NSSL: (1) A special raingauge network in 4 countries, (2) an enhanced pilot balloon network of about 20 temporary additional stations, and (3) a NOAA P-3 Research Aircraft campaign. Although none of these programs concentrated on the altiplano, the SALLJEX still represented a valuable opportunity to sample the region given the larger spatial and temporal density of the temporary observing systems. Given the existing meteorological interest that had been established through the various PACS-SONET and LBA initiated activities, it seemed opportune to enlist the support of the Bolivian meteorological community in a study that might be particularly valuable at the national level. Consequently, several short observational campaigns centered over the altiplano, and particularly over the Lake Titicaca and Salar de Uyuni regions were organized and then carried out. These activities eventually involved the participation of individuals from a number of countries in South America.

A short but more detailed observational campaign was designed for the Altiplano in parallel to SALLJEX activities, as mentioned above. This was done using inexpensive technology (i.e. optical theodolites, digital thermometers, simple raingauges) and maximum participation given the availability of a number of motivated individuals and a limited (~USD 8000.00) budget. The campaign included the deployment of a raingauge network along the entire Altiplano, and the organization of two short 5-7 day field campaigns to measure the circulations and associated convection induced by Lake Titicaca and the Salar de Uyuni. Both campaigns used a network of 5 to 7 pilot balloon stations, surface observations and cloud photography.

Most of the data were successfully collected during the altiplano campaigns with the exception of special Bolivian raingauge measurements, which were never recovered. Additional limitations include the reduced amount of surface observations and the loss of a tethered balloon in transit, which strongly affected the number of thermodynamic soundings that could have been made. The observational component of this study therefore relies on 98 sites of daily rainfall observations located in the vicinity of Lake Titicaca and on high temporal resolution (i.e. 1-hour interval) wind data from the pilot balloon networks. The results are complemented with satellite data and numerical analyses from NCEP's aviation model.

Figure 12. Nocturnal convective storm that developed over the western shore of Lake Titicaca during the PACS-SONET December 2000 Field Experiment. The picture was taken from the Isla del Sol, near the center of the lake, looking west. Note stars in the sky. The picture was taken using a digital camera with long time exposure.

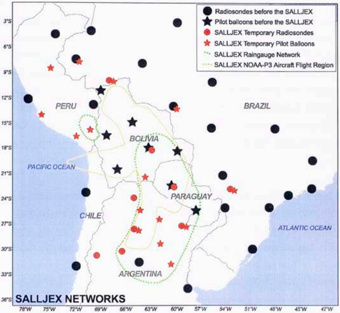

Figure 13. Upper air network available during the SALLJEX. The large black dots are the operational radiosondes sites that were active before and during the experiment. The large black stars are the PACS-SONET pilot balloon sites also active before and during the field campaign. The small red dots represent the temporary radiosonde stations that operated during the SALLJEX. The small red stars correspond to the pilot balloon sites that operated during the SALLJEX. The green thick dotted line represents the region were the raingauge networks were enhanced and the thin orange dotted line the region were the NOAA P3 Research Aircraft flights were completed.

1.4. Objectives and approach

The main goal of the present study is to describe the mesoscale circulations and associated rainfall induced by Lake Titicaca and the Salar de Uyuni. Specific objectives include (1) describing the mesoscale circulations and rainfall induced by Lake Titicaca and Salar de Uyuni, (2) exploring which factors present over the lake and not over the salar favor the development of nocturnal storms, (3) describing and summarizing the interaction between mesoscale and synoptic scale processes that lead to the enhancement and suppression of nocturnal convection, and (4) providing information to start understanding the role of mesoscale processes on the transition from dry to widespread wet conditions in the altiplano.

Towards achieve the above stated goals, both an observational and a short modeling study are developed and presented. Daily surface rainfall data, hourly wind observations from pilot balloons, half-hourly infrared satellite data and analyses constructed with NCEP Global Tropospheric Analyses are analyzed to describe and compare the circulations induced by Lake Titicaca and Salar de Uyuni as well as the associated rainfall. The synoptic conditions associated with lake effect rainfall events are also explored through composite analyses stratified using daily rainfall data and constructed with satellite data and NCEP model analyses. A limited modeling study, carried out using the Weather Research and Forecasting (WRF) model and the numerical analyses as initial and boundary conditions, was designed to explore the role of processes that the spatially and temporally limited observations were unable to describe, especially those that enhance or suppress the development and maintenance of the nocturnal convective storms.

2. DATA

2.1. Rainfall data

The rainfall data consisted of information from 98 daily-measuring SALLJEX raingauges distributed over the Peruvian altiplano (Figure 14), with higher densities along the shores and on the islands of Lake Titicaca. Before the SALLJEX, the spatial density of the operational network in the altiplano was not adequate to resolve sharp mesoscale rainfall gradients such as the ones present near Lake Titicaca. This motivated the design of a temporary altiplano raingauge network based on simple raingauges (Figure 15 and Figure 16) with larger densities in the vicinity of Lake Titicaca and the Salar de Uyuni. The network was established between October and November of 2002 and the data was collected during May and June of 2003. Unfortunately, although a large number of gauges were distributed in Bolivia no data has been received to date from these sites. For this reason the analysis is constrained to the Peruvian side of the altiplano, with an emphasis on the islands, shores and the terrain that surrounds Lake Titicaca. By the end of the campaign, 6 months of daily rainfall observations were available from 116 sites located in the Peruvian side of the altiplano. The Peruvian Weather Service (SENAMHI) provided additional daily rainfall information from 50 stations, some of them located next to the SALLJEX gauges, which served as reference points for the quality control procedures.

The SALLJEX rainfall data were collected by local volunteer observers trained during the installation campaign. To assure the data quality, simple forms and a manual describing the process to measure rainfall were handed out and explained at every site. The team in charge of the network deployment employed 1 to 2 of hours to train each volunteer observer. The forms handed out consisted of drawings of the raingauge, organized daily, where the observers marked the height of the water collected by the instrument (Figure 16). The purpose of this strategy was to reduce the observing errors produced by confusion of the inexperienced observers with the non-linear scale of the gauge.

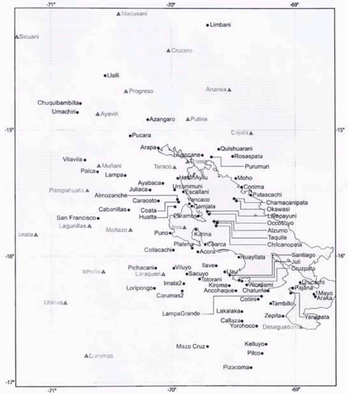

Figure 14. 98-Sites altiplano raingauge network utilized for the analyses. The triangles correspond to SENAMHI stations and the black dots to SALLJEX raingauges. Lake Titicaca is outlined and shaded in light gray. The terrain higher than 4500 m ASL has also been shaded in light gray.

Figure 15. SALLJEX raingauge located in Taquile (island in Lake Titicaca) installed by Teresa Garcia (left) and Carmen Reyes (right) from SENAMHI.

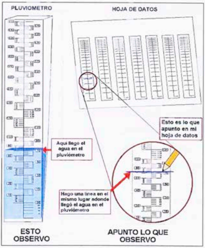

Figure 16. Figure extracted from the SALLJEX raingauge operation manual distributed in the Altiplano. The drawing illustrates the scale of the raingauge and the simplified method suggested for the data registration.

Quality control procedures applied to the rainfall datasets included (1) a comparison of sites in which both a SALLJEX and a SENAMHI raingauge were operated and (2) the use of station-to-station correlations to filter the low-correlated sites. Nevertheless, it should be pointed out that the lack of experience of the volunteer observers should be taken into account. The comparison analysis shows very high correlations (0.94 to ~ 1) for 50 % of the gauges for the co-located sites, and higher than 0.6 for 71% of the pairs. This suggests that the variability of most of the SALLJEX gauges may be related to that of the SENAMHI ones with a small bias on the collected amount. For the station-to-station correlation analysis a correlation matrix was produced and both the station averaged correlation and the number of correlations higher than 0.5 were compared. It is worth mentioning that the convective nature of the altiplano rainfall, together with local variability caused by complex orography, lessens the station-to-station correlation values, especially those from stations separated by large distances. The threshold set for the site selection was (1) averaged correlations higher than 0.10 and (2) a number of at least 3 correlations higher than 0.5. Following this procedure 98 sites (Figure 14) were selected. Finally, the analyses are focused over a 3-month period from 1 December 2002 to 28 February 2003 based on the availability of datasets from other components of the study.

2.2. Upper air data

The analyzed wind data consists of two 5- to 7-day-long datasets of hourly wind profiles from two pilot balloon networks operated in the vicinity of Lake Titicaca and Salar de Uyuni. The data were gathered during two short field experiments carried out in parallel with the SALLJEX field campaign. The first experiment was held in the vicinity of Salar de Uyuni during 25-30 November 2002, and consisted mainly of a network of 5 pilot balloon stations distributed about the salar (Figure 17, upper panel). The distribution of the stations was planned to measure the salar-induced mesoscale circulations, which would provide the low-level divergence estimations to infer the salar-induced vertical motions. Consequently 4 of the stations were located near the edges of the salar, with one in the middle, forming a polygon that gave 4 triangles for the divergence calculations (Figure 17, lower panel). The stations were operated by a team from the National Severe

Storms Laboratory (NSSL); by individuals from different Bolivian institutions including Universidad Mayor de San Andres (UMSA), the Administracion de Aeropuertos y Servicios Auxiliares para la Navegacion Aerea (AASANA), and the Bolivian Weather Service (SENAMHI-Bolivia); and by a supplementary group of 5-10 participants from different South American countries. Hourly soundings were made during the day and 3-hourly during the night with the aid of special night-lights. At the central site frequent surface measurements were made as well as tethered balloon soundings and cloud photography. Due to the limited temporal and spatial resolution of the latter, the analysis has been focused on the pilot balloon information.

The second altiplano experiment was held in the vicinity of Lake Titicaca during the first week of January 2003. It consisted again of a network based mainly on pilot balloon stations for the same reasons as those for the Uyuni network, with 7 stations being distributed along the shores of the lake (Figure 17). Given the position of the Peruvian-Bolivian border across Lake Titicaca, 3 stations lay on Bolivian territory and 4 in Peru. These networks were again operated by the same institutions and by individuals from the Peruvian Weather Service (SENAMHI-Peru). The coordinates of the stations are presented in Table 1.

As with any type of observation, the pilot balloon observations present limitations. The length of the sounding depends on the visibility of the balloon, which is limited by the sky conditions and skill of the observer. Low-level clouds, very strong winds and nighttime darkness are the most common situations that reduce the height of the observed profile. Since all of these conditions were present at different times during the Titicaca and Uyuni experiments, the depth of the wind profiles can vary significantly from one observation to the next. To minimize data gaps, the data were exposed to a linear interpolation in time only whenever 1 or 2 hourly observations were missing, filling some of the gaps present on the dataset, especially in mid- and upper-troposphere. Fortunately at lower levels, were the effects of the salar and the lake airflow are expected to be the largest, not much interpolation was needed as the gaps were concentrated for the most part among the nocturnal 3-hourly observations.

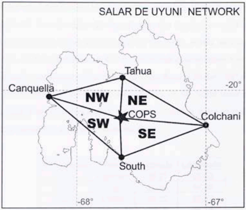

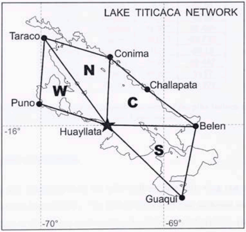

Figure 17. Salar de Uyuni (top) and Lake Titicaca (bottom) pilot balloon networks and polygons used for the divergence estimations. Four triangular regions were analyzed over Lake Titicaca (West, North, Central, and South) and 4 over Salar de Uyuni (NE, SE, SW, E).

For the breeze the diurnal cycle of the 100-200 mAGL onshore and offshore components of the wind were considered since the strength of the breeze signal was the strongest at this level. For the Salar de Uyuni data this implied a zonal and meridional component analysis since the sites were placed by the north, south, east and west shores. For Lake Titicaca, on the other hand, a 40°-counterclockwise-rotation was applied to the zonal and meridional component of the winds to align them with the –40° oriented axis of the lake. The across-lake and along-lake components of the wind were then analyzed. The hourly averages were also exposed to a 3-hourly centered mean to reduce the effects of high frequency variations associated with the flow.

Experiment	Station	Latitude	Longitude
Uyuni	Colchani	-20.27	-67.03
Uyuni	South	-20.44	-67.66
Uyuni	COPS	-20.22	-67.67
Uyuni	Canquella	-20.08	-68.19
Uyuni	Tahua	-19.96	-67.65
Titicaca	Guaqui	-16.583	-68.85
Titicaca	Huayllata	-15.997	-69.465
Titicaca	Belen	-16.017	-68.733
Titicaca	Challapata	-15.7	-69.15
Titicaca	Conima	-15.455	-69.442
Titicaca	Taraco	-15.293	-69.97
Titicaca	Puno	-15.822	-70.008

Table 1. Latitude and longitude (in degrees north and west) of the pilot balloon stations operated during the Lake Titicaca and Salar de Uyuni Field Experiments.

2.2.1. Divergence calculations

Divergence was computed from the pilot balloon data following one of the methods described by Davies-Jones (1993). The author compared four different methods applied for the calculation of divergence and vorticity by utilizing wind profiles. He showed them to be equivalent when using data from a network of three non-collinear stations since all of the methods are based on the assumption of a linear wind field. He concluded that the most simple but also most efficient method was fitting a linear velocity field to the observed wind components. The main advantage of this method arises from the fact that a

2 x 2 system of algebraic equations are produced yielding a simple analytical formula for the calculation of divergence. This method was utilized for the estimation of divergence over Lake Titicaca and Salar de Uyuni, and will be consequently described.

Consider the (x_i, y_i) to be the conventional distance coordinates of an observation point i, and (u_i, v_i) the corresponding wind components. For a subset of 3 stations, the fitting method consists of finding the planes through the three points (x_i, y_i, u_i) in x-y-u space and through three points (x_i, y_i, v_i) in x-y-v space (Pedder, 1981; Davies-Jones, 1993). The wind can be decomposed into a linear velocity field of the form:

$$u = u_o + ax + by, \quad v = v_o + cx + dy \qquad (1)$$

where $a=\partial u/\partial x$, $b=\partial u/\partial y$, $c=\partial v/\partial x$ and $d=\partial v/\partial y$ are considered to be constants over the region spanned by the three points. The constants u_o and v_o depend on the arbitrary location of the origin of the coordinate system. The vector (u_o, v_o) will represent the mean windfield when the centroid (located by the mean position vector) is chosen as the origin (Endlich and Clark, 1963; Davies-Jones, 1993). For an analysis constructed with 3 stations, the linear system governing a and b becomes

$$(x_2 - x_1)a + (y_2 - y_1)a = u_2 - u_1, \qquad (2a)$$

$$(x_3 - x_1)a + (y_3 - y_1)a = u_3 - u_1, \qquad (2b)$$

(Endlich and Clark, 1963; Davies-Jones, 1993), and the one for c and d becomes

$$(x_2 - x_1)c + (y_2 - y_1)d = v_2 - v_1, \qquad (3a)$$

$$(x_3 - x_1)c + (y_3 - y_1)d = v_3 - v_1, \qquad (3b)$$

The solutions using Cramer's rule (Davies-Jones 1993) are:

$$a = \frac{\begin{vmatrix} u_2 - u_1 & y_2 - y_1 \\ u_3 - u_1 & y_3 - y_1 \end{vmatrix}}{2\,A(0)} \qquad b = \frac{\begin{vmatrix} x_2 - x_1 & u_2 - u_1 \\ x_3 - x_1 & u_3 - u_1 \end{vmatrix}}{2\,A(0)}$$

$$c = \frac{\begin{vmatrix} v_2 - v_1 & y_2 - y_1 \\ v_3 - v_1 & y_3 - y_1 \end{vmatrix}}{2\,A(0)} \qquad d = \frac{\begin{vmatrix} x_2 - x_1 & v_2 - v_1 \\ x_3 - x_1 & v_3 - v_1 \end{vmatrix}}{2\,A(0)}$$

and

$$A(0) = \frac{1}{2}\begin{vmatrix} 1 & x_1 & y_1 \\ 1 & x_2 & y_2 \\ 1 & x_3 & y_3 \end{vmatrix} = \begin{vmatrix} x_2 - x_1 & y_2 - y_1 \\ x_3 - x_1 & y_3 - y_1 \end{vmatrix}$$

where ***A(0)*** is the area of the triangle formed by the stations (Gellert et. al, 1977).

The distances between the stations were estimated using a relationship of 111 km $deg(lat)^{-1}$ and 105 km $deg(lat)^{-1}$ for the longitude and latitude variations respectively, due to the effects of the curvature of the earth. A list containing the latitudes and longitudes of the stations are displayed in Table 1.

2.3. Satellite data

Satellite composites were constructed using GOES-8 infrared satellite data provided by the UCAR Joint Office of Science Support (JOSS). The data have a horizontal resolution of 4km and a temporal resolution of 30 minutes, leading to 48 frames to describe the diurnal cycle of convection. Even though the direct relationship between rainfall and cloud top temperature is quite complex, this tool was found useful to describe the basin-wide distribution and evolution of the cold clouds, and in particular the diurnal cycle, since the raingauge network provided only daily rainfall data. Firstly, cloud top temperature information was obtained by transforming the GOES-8 IR4 brightness (Mode-A counts) data into temperature using the conversion table 5-1a provided by Weinreb et al. (2001). Secondly, the frequency of convective clouds was evaluated at different levels by analyzing the cloud top temperatures colder than different temperature thresholds. Timeseries of daily averages obtained from these calculations were correlated with the lake station rainfall observations measured at the corresponding pixels to identify the temperature thresholds at which the correlations were the highest (Figure 18). It was found that the highest correlations between cold cloud frequency and convection over Lake Titicaca occur when the frequency of clouds colder than ~ –13°C is analyzed. The averaged correlations were, however quite low (< +0.3) due to the local and short-lived nature of the altiplano rainfall, and due to the frequent presence of cirrus clouds originating from afternoon convection or nocturnal convection along the eastern slopes of the Andes. Taking these factors into account, the threshold used for the Lake Titicaca region convection analysis was –15°C.

A composite analysis of days in which lake-effect storm events occurred (hereafter, LESD's) versus days in which these events were weak or not present (hereafter, NLESD's) was constructed stratifying the satellite data and numerical analyses described in section 2.4 based on the rainfall observations. The period of analysis was constrained to three months of observations between 1 December 2002 and 28 February 2003, based on the availability of the satellite data and numerical analyses. From the 90 days of rainfall observations, the LESD's were considered as the 30 cases with the largest positive differences between the rainfall collected by the lake stations minus the ones collected by the land stations (Figure 19). In contrast, the NLESD's were considered as those 30 cases with the largest negative differences likewise calculated. The selected land stations were those 37 sites located among the Altiplano basin, which were at least 20 km away from Lake Titicaca, whereas the lake stations were those 30 sites located either on the islands or onshore at a distance not larger than 5 kilometers away from the lakeshore and that received 400 mm or more during the period of analysis. Daily rainfall observations averaged over all the lake stations are compared with those averaged over the land stations and presented on a scatterplot (Figure 20).

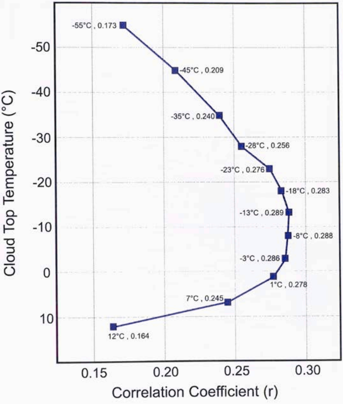

Figure 18. Averaged correlations between the GOES-8 derived daily-averages of cold cloud frequencies and rainfall measured by the lake stations.

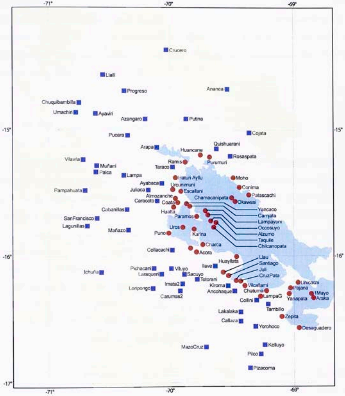

Figure 19. Lake stations indicated with red dots and land stations indicated with blue squares. The elevations above 4500 mASL is shaded in light brown and Lake Titicaca shaded with light blue.

The diurnal cycle of convection was constructed by calculating half-hourly composites of cold cloud frequencies over the entire Altiplano using IDL. Then the diurnal cycles of cold cloudiness for (1) LESD's and (2) NLESD's were constructed. The seasonal diurnal cycle was subtracted to visualize the departure of the cold cloud temperature frequencies from the seasonal average and characterize the convection during both LESD's and NLESD's.

2.4. NCEP Global Tropospheric Analyses

These are gridded analyses that cover the world every 6 hours prepared by the NCEP Final Global Data Assimilation System (FNL). The data in the analyses are organized on grids with a horizontal resolution of 1 degree and 26 pressure levels in the vertical. The variables contained are surface pressure, sea level pressure, geopotential height, temperature, sea surface temperature, ice cover, relative humidity, zonal wind, meridional wind, vertical velocity, vorticity and ozone content. The FNL system collects observations from at least 6 hours past synoptic time ingesting a larger number of observations, which are exposed to spectral statistical interpolation to obtain the numerical analyses (Parrish and Derber, 1992). The model grid has a resolution of T254L64. This implies that the horizontal resolution is roughly 55km. The vertical resolution is higher at lower levels and approximates a 680-meter mesh at 250 mb.

Following the methodology applied to the satellite imagery dataset, the seasonal averages were computed, then the analyses were stratified on LESD's and NLESD's, and finally the seasonal mean was subtracted to depict the variations of the synoptic flow associated with nocturnal convective events over Lake Titicaca. Instead of describing the diurnal cycle of the wind anomalies, the analysis was constructed with daily analyses centered at 12 UTC.

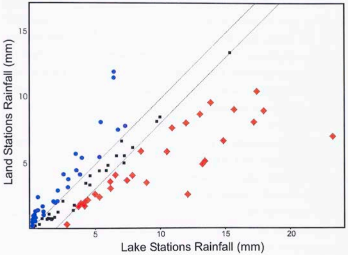

Figure 20. Scatterplot constructed with the rainfall averaged over the lake stations (x-axis) versus the rainfall averaged over the land stations (y-axis). The 30 cases selected as LESD's are indicated with red diamonds and the NLESD's with red circles. The small black squares represent the 30 intermediate cases, neglected for the composite analyses.

3. OBSERVATIONAL STUDY OF THE ALTIPLANO MESOSCALE CIRCULATIONS

3.1. Satellite perspective of the altiplano cloudiness

The diurnal cycle of clouds colder than –15°C calculated over the 01 December – 28 February 2002-3 period is presented in Figure 21. As described in previous studies, widespread convection over land starts around noon (panel b), peaks during the late afternoon and early evening (panel c) and fades after this period with a localized maximum over Lake Titicaca from 20 LST through 08 LST (panels d, e and f) associated with nocturnal convective storms. Remnants of the cloudiness associated with these storms are still evident during the morning (panel a), which is the period of less frequent convective activity over the altiplano. Afternoon convection appears to be more frequent from these analyses than nocturnal convection over the lake, with frequencies in the range of 20 to 60% in the northern altiplano during the afternoon versus 20 to 40% over Lake Titicaca during the night. The diurnal effects of Lake Titicaca and the Salar de Uyuni on the cloud field are also evident, especially in panels b and c, where regions of lower cold cloud frequencies are located over both features. The cold cloud frequency difference between land and lake ranges between 30-50% over land versus 10-20% over the lake between 12 and 16 LST, and from 6-20% over the terrain that surrounds the salar versus 2-6% over the salar. Nocturnal convection over the salar is not present according to these analysis.

The northeast/southwest cloudiness gradient associated with the moisture distribution over the altiplano is evident from Figure 21. Whereas diurnal frequencies on the order of 20-60% occur in the northern altiplano during the afternoons, frequencies on the order of 6-20% are observed in the southern altiplano. A limitation of this analysis is the noise introduced by cirrus clouds from altiplano convection or from convection produced over the eastern slopes of the Andes during the night, which lower the correlations between cold cloudiness and rainfall as discussed in section 2.3.

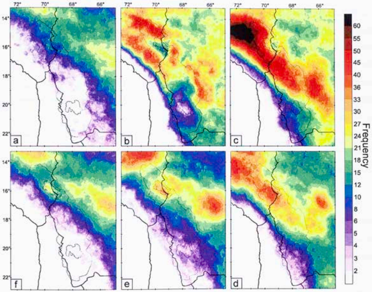

Figure 21. Diurnal cycle of convection as seen from the seasonal (December-February 2002-3) frequency of clouds colder than –15°C calculated for (a) 08-12 LST, (b) 12-16 LST, (c) 16-20 LST, (d) 20-00 LST, (e) 00-04 LST, and (f) 04-08 LST.

3.2. Analysis of rainfall

Concomitant with the period selected for the satellite analysis, the observed rainfall was averaged over the 1 December – 28 February 2002-3 period and is displayed in Figure 22. The analysis clearly shows that the region of largest rainfall is located over Lake Titicaca, in particular towards the northeastern portion of the lake with 3-month accumulations as high as 636 mm (212 mm month^{-1}) on the southern tip of Isla Soto, located in the northeastern part of the Lake. Since the convection over Lake Titicaca occurs during the night, as suggested by diurnal cycle of cold clouds averaged over the season (Figure 22), the combined results suggest that this maximum is indeed associated with nocturnal lake effect storms. The associated mesoscale circulations involved in the generation of these storms will be discussed in the next section. A relative rainfall minimum of ~200-350 mm (~70-115 mm month^{-1}) is also evident along a ~50 km-wide strip inland from the shores of Lake Titicaca, and a secondary maximum farther inland over the mountainous terrain. The latter maximum, associated with afternoon convection according to the satellite climatologies, is associated with upslope terrain-induced breezes generated during the day.

Although satellite imagery (Figure 21) suggests that the region of the most frequent convection occurs in the central-western part of Lake Titicaca, near the island of Taquile, the observations indicate that the region of largest rainfall is displaced east-northeast from the region of maximum convection. This may be related to the vertical structure of the flow over Lake Titicaca during lake-effect-storm days, which is weak and convergent at lower levels and has an easterly component in the levels where the cloud tops occur, as will be discussed the sections that follow. It is also noticeable from the satellite analysis that the frequencies of cold clouds are larger during the afternoon than during the night, which would suggest larger rainfall rates over land than over the lake. The rainfall observations, however, indicate the contrary. This situation suggests that non-explored factors such as dry air entrainment and microphysical processes may be playing a role on the production of larger rainfall rates over the lake and should be explored with detail with a future study.

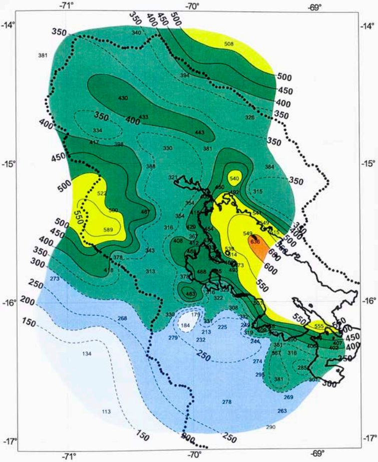

Figure 22. Rainfall (in mm) accumulated during the 1 December 2002 – 28 February 2003 period by the 98-site raingauge network. Lake Titicaca is indicated with a thick solid black line and the edge of the Altiplano basin with a dotted line.

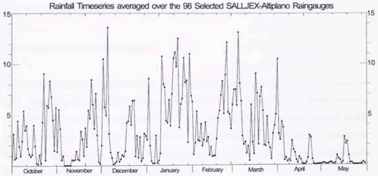

Figure 23. Rainfall timeseries (in mm) product of averaging over the 98-site raingauge network.

The temporal evolution of rainfall over the Lake Titicaca area was also explored and plotted in Figure 23. As expected according to the literature, the core of the rainy season occurred between January and March with 11 days during which the rainfall averaged over all the stations exceeded 10 mm. Several dry spells associated with periods of mid-tropospheric westerly flow with durations of 5 days to 3 weeks were present. Unfortunately, the Lake Titicaca Field experiment coincided with one of these events, which were favorable for pilot balloon observations given the reduced cloudiness but biased the analysis towards circulation patterns associated with dry conditions.

3.3. Salar de Uyuni field experiment

3.3.1. Observational campaign

The Salar de Uyuni observational campaign was carried out during 25-30 November 2002, parallel to the SALJJEX field activities. About 40 participants from South America and the United States, but mainly from Bolivia, were involved. The team arrived in the salar on November 25th and was distributed among the five observing sites illustrated in Figure 17, with a larger concentration on the central site given the larger number and types of observations carried out in this location.

The core of the observational campaign were hourly pilot balloon wind measurements carried out using optical theodolites and inflating the balloons with helium. Nocturnal soundings were also made with the aid of special night-lights, however following the balloons was not easy given the windy conditions which resulted in short lived soundings. The nocturnal soundings were made with a 3-hourly frequency but unfortunately many gaps in the dataset complicated the nighttime analysis.

Additional observations made at the Salar included daily maximum and minimum temperature observations at 8 locations, a reduced number of tethersonde observations in the central station, cloud photography at 2 locations, surface temperature measurements at three levels at the five stations, and temperature/dewpoint/solar radiation observations in the center of the salar. The number and depth of the thermodynamic soundings were affected by the windy conditions, and some of the surface data was not recovered. For these reasons, the analysis is centered on the pilot balloon wind profiles.

3.3.2. Structure and diurnal variation of the salar breeze

The wind maps plotted on Figure 24 summarize the low-level (100-200 mAGL) circulations observed over the Salar de Uyuni during the field campaign. The 100-200 layer was used since the effects of the salar airflow are the strongest in the lowest levels of the atmosphere. Early morning confluence is not evident from these maps contrasting with evident diffluence during the early afternoon, with the largest wind observation (~7.5 m s^{-1}) measured in the southernmost site. The arrival of flow generated apparently over the western slopes of the Andes (hereafter, western slope flow or WSF) was observed.

The diurnal cycle of the winds perpendicular to the coasts is summarized in Figure 25. The most remarkable feature present in these figures is the arrival of strong westerly flow in the afternoons as evidenced by the zonal component displayed on the lower panel. This indicates that the strongest flow occurs in the westernmost site with a zonal component of ~ +16 m s^{-1} and decreases towards the easternmost location to a zonal component of ~ +7 m s^{-1} near the time of the strongest winds. Channeling effects produced by the gaps in the western slopes that weaken as the flow expands over the wide and flat salar may explain this type of flow pattern, however the observations available can only suggest, not describe, such events.

The breeze signal was extracted by removing the all-station mean and is presented in Figure 26. The analyses shows a clear signal of the breezes during the day, especially when comparing the west and east sites. The amplitude of the onshore breezes ranges from 1 to 2 m s^{-1}. The strongest breeze was observed, again, in the southernmost location

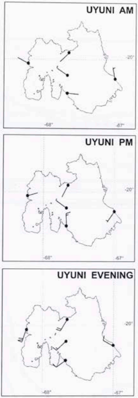

Figure 24. 100-200 mAGL winds averaged over the Salar de Uyuni experiment plotted for different times of the day. The top panels represent the early morning winds corresponding to the hour of maximum convergence (07 LST). The central panel illustrates the winds corresponding to the hour of maximum divergence (13 LST). The bottom panels correspond to the periods with the strongest winds (19 LST) due to the arrival of diurnally-generated upslope flow in the western slopes of the Andes. The wind barbs are in knots.

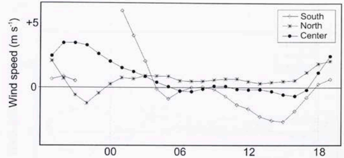

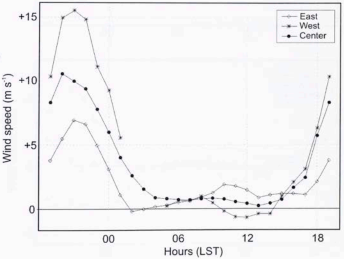

Figure 25. Diurnal cycle of the meridional component of the wind (top) and the zonal component (bottom) averaged over the 100 – 200 mAGL layer and over 5 days of observations during the Salar de Uyuni experiment. The information from the 3 sites located in the north-south transect is presented in the top panel and in the bottom panel the information from the 3 sites located in the east-west transect. A 3-hour centered mean was applied to smooth the timeseries. The winds are in m s^{-1}.

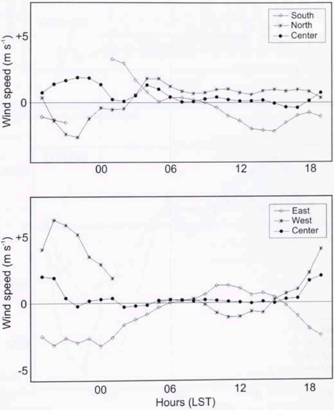

Figure 26. Same as prior figure but with the all-station mean removed in order to filter the effects of the large scale circulation. This analysis provides a clearer signal of the onshore and offshore breezes. The winds are in m s^{-1}.

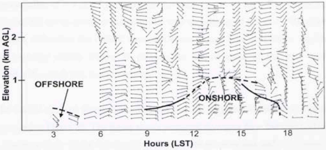

Figure 27. Diurnal cycle of the wind anomalies with respect to the all-station mean observed on the southern shore of the Salar de Uyuni.

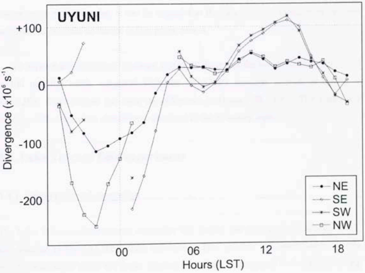

Figure 28. Diurnal cycle of divergence in the 100-200 mAGL layer calculated over Salar de Uyuni for the 4 regions illustrated in Figure 17 using the experiment-averaged wind observations after a 3-hour centered mean pass. The divergence is in 10^6 s^{-1}.

with magnitudes of ~ 3 m s^{-1} that persisted between 13 and 15 LST. The breeze signal was present but not as strong at the north site with magnitudes of ~ 1 m s^{-1}. The depth of the breezes, defined as the vertical extension above ground level at which a significant diurnal variation ceases. Figure 27 presents the diurnal cycle of the wind profiles measured at the south site, as an example.

The diurnal cycle of divergence calculated over the polygons illustrated in Figure 17 are presented in Figure 28. The figure shows persistent divergent flow from 05 LST to 17 LST. The magnitude of the divergence during the late morning and early afternoon was on the order of +100 $x10^{-6}$ s^{-1}. During the evening, however, strong convergence associated with the arrival of the WSF occurs. Values as large as ~-250 $x10^{-6}$ s^{-1} occur in the northwestern quadrant of the salar. Since the WSF appeared to be the only source of convergence over the salar, it can be argued that the salar-induced circulations are not sufficient to generate nocturnal convergence over it.

To support the divergence findings, Figure 29 illustrates the low-level (i.e. 630 mb or ~ 300 mAGL) winds measured with the NOAA-P3 research aircraft at during a SALLJEX flight carried out over the Altiplano in January 28, 2003. The winds are strongly diffluent and no clouds were observed in the boundary layer.

3.4. Lake Titicaca field experiment

3.4.1. Observational campaign

The Lake Titicaca observational campaign was carried out during 02-09 January 2003, also parallel to the SALJJEX field activities. The number of participants on this activity was larger given the larger number of stations, 7 compared to 5 stations during the Uyuni experiment (Figure 17) and the closeness of the sampling locations to the city of La Paz, home of most of the participants. The team was composed by ~50 South Americans, mainly Bolivian and a small group of Peruvians, who arrived in the region

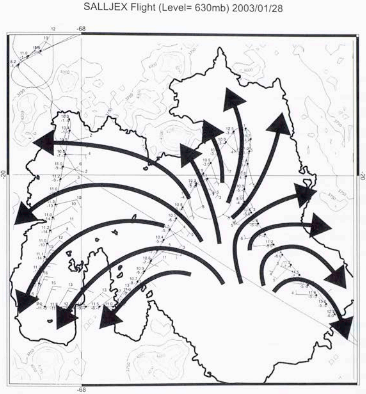

Figure 29. Low-level (630 mb) winds and streamlines showing highly diffluent and divergent flow over Salar de Uyuni measured by the NOAA-P3 research aircraft NEAR 11 LST January 28, 2003. The plotted winds are in knots.

between December 28 and January 2nd. The observational campaign started in January 3rd and ended on January 9th.

The operations center was this time located in the city of Puno, to the northwest of the Lake, and the largest number of observations were carried out in Huayllata, located on the central-western shore of Lake Titicaca, both on the Peruvian side. Similarly to the Uyuni experiment, the analysis was mainly focused on the pilot balloon wind observations based on the completeness of the dataset. Nocturnal observations were also made with a 3-hourly frequency, but in this case the winds were weaker therefore the soundings were deeper and the nocturnal data set more complete when compared to that collected at the Salar de Uyuni.

Additional observations include 1.5 meter temperature observations with a 15-minute frequency in each of the sites, cloud photography and temperature/dewpoint/solar radiation data from a surface meteorological station based in Huayllata. Thermodynamic profiles were not collected with the desired frequency since the tethersonde was lost in transit, but a reduced number (~5) of radiosonde soundings were made.

3.4.2. Structure and diurnal variation of the lake breeze

Figure 30 shows a comparison between the early morning, near noon and evening 100-200 mAGL circulations averaged over the Lake Titicaca and Salar de Uyuni experiments. Morning confluent flow was evident from the observations over the lake but not over the salar whereas diffluent flow was observed over both features during the early afternoon. A remarkable process (hereafter, eastern slope flow or ESF for Lake Titicaca) observed every late-afternoon and evening, summarized in the bottom panel of Figure 30, is the arrival of foreign (i.e. generated outside from the altiplano) air masses from eastern slopes into the Lake Titicaca region, a similar process to the one observed over the salar.

The diurnal cycle of the winds perpendicular to the coasts is summarized in Figure 31. The all-station mean winds were subtracted to isolate the breeze signal from the large-scale circulation and the results are presented on Figure 32. The onshore component of the circulation associated with the lake breezes is present at every site during the late morning and early afternoon, being less evident in Belen and less prolonged at Challapata. The diurnal cycle observed at Belen is the product of the orientation of the bay where the station was established, which induces a 90° angle between the nocturnal offshore and the diurnal onshore breezes not captured by this analysis (see the top panel of Figure 30). An offshore component of the circulation prevails in most locations, again with the exception of Challapata, from 17 LST to 08 LST. The effects of the ESF, however, mask the effects of the diurnal variability associated with the lake, especially during the 19 – 03 LST period. The magnitude of the onshore circulations was weak and found to vary between 1 and 2 m s^{-1} and does the one of the offshore circulations in most of the stations. The ESF produces wind speeds larger than 4 m s^{-1}, as observed in Conima.

The depth of the breezes was also explored. Figure 33 show the diurnal cycle of the wind profiles measured at Belen (top) and Conima (bottom) and indicate a clear onshore signal between 09 and 15 LST. The observations suggest that the onshore flows exhibits depths that vary between ~700-1400 mAGL with the maximum vertical extension observed near local noon (17 UTC). The nocturnal offshore flow, present at both stations, is masked by the arrival of the upslope flow in the afternoon, especially in Conima, where deeper nocturnal offshore flows occur.

The particular features observed in the afternoon and nocturnal Challapata averages were not a product of a single period of erroneous measurements but were present on a daily basis. Furthermore, the winds in upper layers (i.e. above 1000 mAGL) were spatially and temporally coherent, which suggests that these particularities may be real and the product of a locally induced mesoscale process. Given resolution of the network this hypothesis cannot be verified.

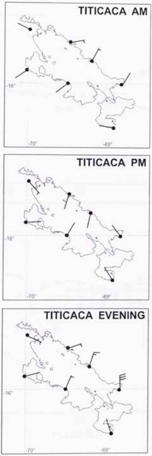

Figure 30. 100-200 mAGL winds averaged over the Lake Titicaca experiment plotted for different times of the day. The top panels represent the early morning winds corresponding to the hour of maximum convergence (05 LST). The central panel illustrates the winds corresponding to the hour of maximum divergence (12 LST). The bottom panels correspond to the periods with the strongest winds (18 LST) due to the arrival of diurnally-generated upslope flow in the eastern slopes of the Andes. The wind barbs are in knots.

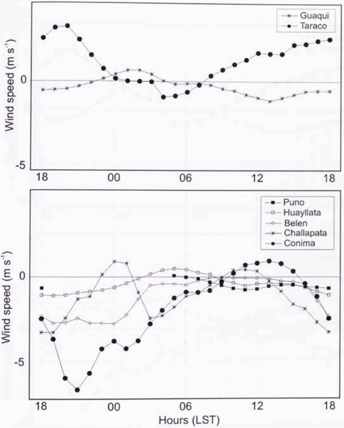

Figure 31. Diurnal cycle of the rotated-along-lake component of the wind (top) and the rotated-across-lake component (bottom) averaged over the 100–200 mAGL layer and over 7 days of observations during the Lake Titicaca experiment. The information from the two sites located at opposite ends of the lake (Taraco to the north and Guaqui to the south) are presented in the top panel. The information from the 5 sites located in the west (Puno and Huayllata) and east (Belen, Challapata and Conima) coasts of the lake are presented in the bottom panel. A 3-hour centered mean was applied to smooth the peaks product of a too short sampling period. The rotation applied was 40° counter-clockwise. The winds are in m s^{-1}.

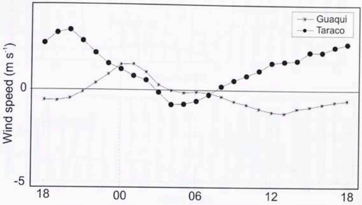

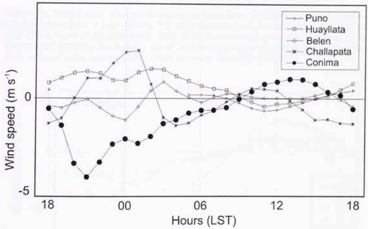

Figure 32. Same as prior figure but with the all-station mean removed in order to filter the effects of the large scale circulation. This analysis provides a clearer signal of the onshore and offshore breezes. The winds are in m s^{-1}.

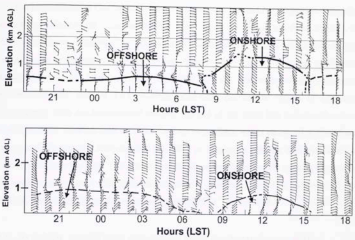

Figure 33. Diurnal cycle of the winds observed at Belen (top) and Conima (center), located on the northeastern shore of Lake Titicaca. The barbs represent the horizontal winds in ms^{-1} and the solid lines a sketch of the approximate depth of the breezes based on the windshift height. The bottom panel illustrates the diurnal cycle of the wind anomalies with respect to the all-station mean observed on the southern shore of Salar de Uyuni. The winds are in knots.

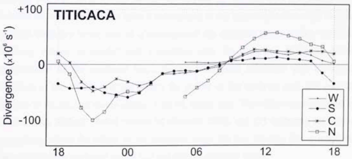

Figure 34. Diurnal cycle of divergence in the 100-200 mAGL layer calculated for 4 regions located over Lake Titicaca using the experiment-averaged wind observations after a 3-hour centered mean pass. A map illustrating the location of the sectors considered for the calculations is displayed in Figure 17. The winds are in m s^{-1}.

The local effects at Challapata described above were ignored for simplicity during the divergence calculations. The results for 4 polygons: W (Huayllata-Puno-Taraco), N (Huayllata-Taraco-Conima), C (Huayllata-Conima-Belen) and S (Huayllata-Belen-Guaqui) are presented in Figure 28 (top panel). They clearly indicate widespread divergence over the lake between 9 LST and 16 LST, and widespread convergence between 20 LST and 04 LST. Counter-intuitively, the largest values of nocturnal convergence were not encountered towards the end of the night but before and around midnight. This, coupled with stronger easterly across-lake winds observed at Huayllata, Belen and Challapata, indicate that the ESF is playing a role in the generation of convergence over the lake. The greatest amplitude of the diurnal cycle appears to occur in the northernmost sector with divergence values as high as $\sim+60\times10^{-6}\ s^{-1}$ between 12 and 13 LST, and convergence values as low as $-100\times10^{-6}\ s^{-1}$ around 21 LST.

3.5. Synoptic conditions associated with nocturnal convection

The synoptic conditions associated with the development of nocturnal convective events and their suppression are explored using the composite analyses for LESD's and NLESD's constructed with the satellite imagery and the NCEP global tropospheric analyses. The 550 mb level was selected to compare the analyses with the rainfall fields and cold cloud anomaly fields since it corresponds to the layer located near and over the altiplano boundary layer, and as a consequence the moisture levels of this layer are positively related to rainfall and convection over the altiplano. Problems in the representation of the mountain range given its steepness combined with the coarse resolution of the NCEP analyses reduce the quality of the analyses over and near the altiplano in the form of waves aligned with the topography. This effect can be filtered by (1) analyzing anomaly fields instead of observed fields and (2) exploring the upper-troposphere, where the effects of the mountain range felt less. Having this in mind, the discussions below are based on the 550 and 400 mb anomaly fields.

Figure 35 shows the characteristic rainfall field for a LESD. The rainfall analysis indicates, as expected, that the region of the largest rainfall rates (> 12 mm day^{-1}) is located over the northern portion of Lake Titicaca surrounded by areas of lower rainfall (4-8 mm day^{-1}) over the land north and northwest off the lake. The lowest rainfall during these events was found to the southwest of the lake with rates lower than 4 mm day^{-1}. On the other hand, during NLESD's (Figure 36) the region of the largest rainfall rates occurred over the western mountain range with rates that vary between 4 and 6.4 mm day^{-1}, versus areas of rates below 2 mm day^{-1} encountered, as expected, over the lake.

The cold cloud anomaly fields associated with the LESD's are plotted in Figure 37. They suggest higher frequencies of convection in most of the Altiplano, especially south of the lake, and also along the eastern slopes during the morning and afternoon prior to the nocturnal convective events. These results coincide with the 550 mb positive moisture anomalies found in this region of the altiplano in the NCEP analyses displayed in Figure 38. The NCEP composites indicate a southeasterly wind anomaly over the southern portion of the region which increases from ~0.5 m s^{-1} over Lake Titicaca to ~3 m s^{-1} over the southern end of the basin, near the Bolivian-Chilean-Argentinean borders (23°S). The geopotential height and temperature anomalies were also explored (Figure 39). They indicate a region of above-normal heights (> 7 m) and warmer temperatures (> 1°C) over and offshore from central Chile, and a region of below-normal heights centered in northern Bolivia. Cooler temperatures over and just east of the altiplano are also consistent with the enhanced convection observed on the satellite imagery, a process that cools the mid-troposphere by injecting low-level air through vertical mixing processes. Furthermore, cyclonic vorticity anomalies to the northeast of the altiplano can be associated with rising motion and therefore enhanced convection in the central and southern Altiplano.

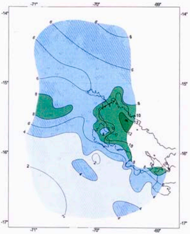

Figure 35. Daily rainfall in mm averaged over the LESD's. Lake Titicaca is indicated with a solid black line.

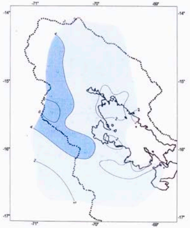

Figure 36. Daily rainfall in mm averaged over the NLESD's. Lake Titicaca is indicated with a solid black line and the edge of the basin with a dotted line.

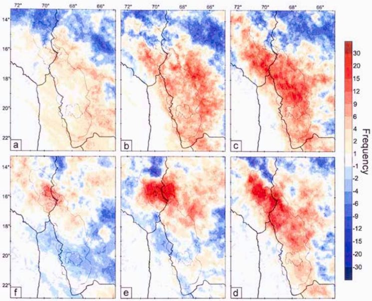

Figure 37. Anomaly of the frequency of clouds colder than –15°C with respect to the seasonal average calculated for the LESD's. The panels present the frequency anomalies averaged over (a) 08-12 LST, (b) 12-16 LST, (c) 16-20 LST, (d) 20-00 LST, (e) 00-04 LST, and (f) 04-08 LST.

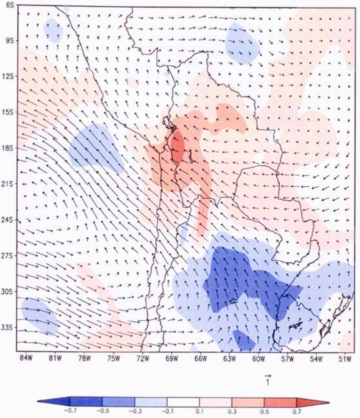

Figure 38. Anomaly of the horizontal wind (vectors) and mixing ratio (shaded) fields at 550 mb during LESD's constructed using the NCEP global tropospheric analyses. The winds are expressed in ms^{-1} and the mixing ratio in g kg^{-1}.

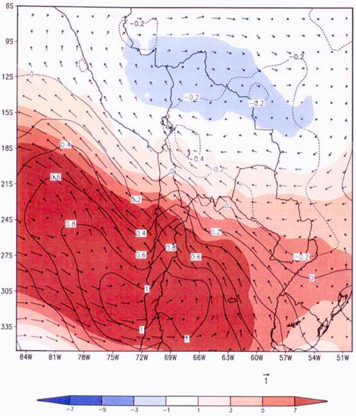

Figure 39. Anomaly of the horizontal wind (vectors), temperature (contours) and geopotential height fields (shaded) fields at 550 mb during LESD's constructed using the NCEP global tropospheric analyses. The winds are expressed in ms^{-1}, the temperature in °C and the geopotential heights in m.

Warmer temperatures (°C) and lower moisture contents (-0.5 to –0.1 g kg^{-1}) over and east of the altiplano coupled with near-normal wind conditions at 550 mb are associated with the NLESD's (Figures 40 and 41). During these events, a region of below-normal geopotential heights at 550mb is present over the South Pacific Anticyclone centered at 24-27°S and west of 84°W, whereas a region of above-normal geopotential heights is observed just east of the altiplano associated with an anticyclonic vorticity anomaly and anomalous sinking motions. These results were also consistent with the NLESD's convection anomaly composite (Figure 42) and the observed rainfall, which indicate below-normal convection near and south of the lake. Since westerly (easterly) flow anomalies at upper levels suppress (enhance) the intensity of the upslope breezes over the eastern slopes of the Andes, the main moisture source of the region, the composite analysis suggests that most of the moisture during the LESD's originates to the southeast of the Altiplano, not to the northeast.

The signals of the anomaly fields encountered at 400 mb were consistent with those found at 550 mb. The 400 mb wind and moisture anomaly fields for the LESD's are presented in Figure 43 and for the NLESD's in Figure 44. They still indicate a southeasterly flow and a cyclonic anomaly over the central and southern altiplano coupled with positive moisture anomalies during LESD's and easterly flow and anticyclonic anomaly over the northern altiplano coupled with negative moisture anomalies during NLESD's. The observed wind and mixing ratio fields characteristic of LESD's are presented in Figure 45. They illustrate the dominant westerly flow over the salar region combined with low mixing ratios. The persistent low moisture content in this sector of the altiplano seems to be the main factor involved in the lack of nocturnal convective storms over the Salar de Uyuni, absent even during the evening when large values of low-level convergence occur. It is worth mentioning that mid-tropospheric westerly flow enhances the advection of dry air masses from over the Pacific, which further reduce the moisture content of the southern altiplano boundary layer during the afternoons. The analysis also indicates south to southwesterly flow at 550 mb over the rest of the altiplano which suggests that the moisture inflow through the gaps in the eastern slopes of the Andes favored mainly by a weakening of the mid-tropospheric westerly/southwesterly flow instead of a reversal of the circulation, or that rainy days are not critically dependent on the wind direction but other conditions.

The convection anomaly composites indicate the regions with the largest positive (negative) convection anomalies occur between 20 and 04 UTC over Lake Titicaca during the LESD's (NLESD's) events, supporting the section 3.1 findings, which indicate that the maximum convective activity over the lake occurs at this time of the day. Furthermore, these results are also consistent with the low-level divergence results obtained with the pilot balloons, which show the period of the maximum convergence between 20 and 04 UTC.

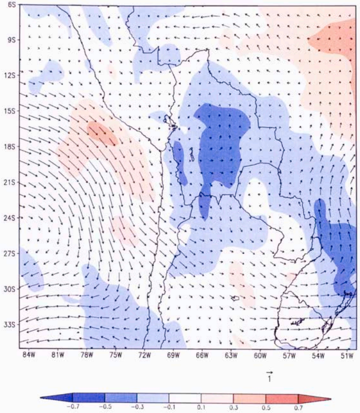

Figure 40. Anomaly of the horizontal wind (vectors) and mixing ratio (shaded) fields at 550 mb during NLESD's constructed using the NCEP global tropospheric analyses. The winds are expressed in ms^{-1} and the mixing ratio in g kg^{-1}.

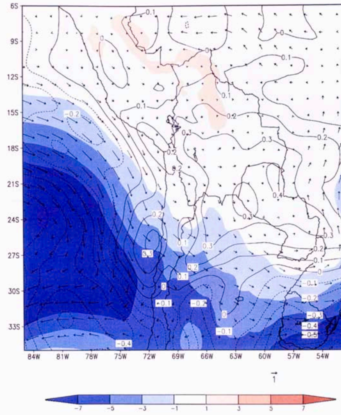

Figure 41. Anomaly of the horizontal wind (vectors), temperature (contours) and geopotential height fields (shaded) fields at 550 mb during NLESD's constructed using the NCEP global tropospheric analyses. The winds are expressed in ms^{-1}, the temperature in °C and the geopotential heights in m.

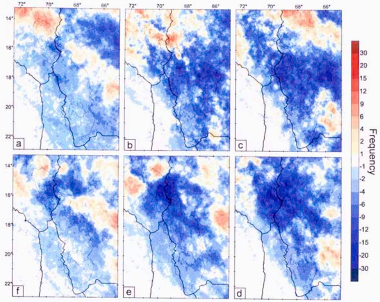

Figure 42. Anomaly of the frequency of clouds colder than –15°C with respect to the seasonal average calculated for the NLESD's. The panels present the frequency anomalies averaged over (a) 08-12 LST, (b) 12-16 LST, (c) 16-20 LST, (d) 20-00 LST, (e) 00-04 LST, and (f) 04-08 LST.

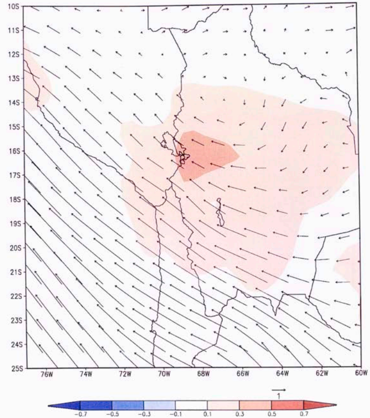

Figure 43. Anomaly of the horizontal wind (vectors) and mixing ratio (shaded) fields at 400 mb during LESD's constructed using the NCEP global tropospheric analyses. The winds are expressed in ms^{-1} and the mixing ratio in $g\ kg^{-1}$.

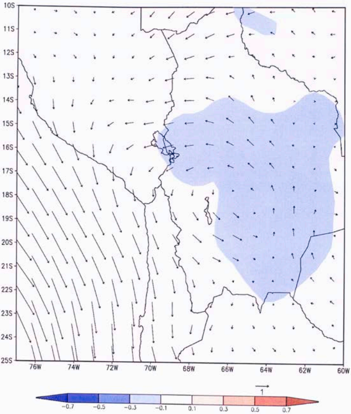

Figure 44. Anomaly of the horizontal wind (vectors) and mixing ratio (shaded) fields at 400 mb during NLESD's constructed using the NCEP global tropospheric analyses. The winds are expressed in ms^{-1} and the mixing ratio in $g\ kg^{-1}$.

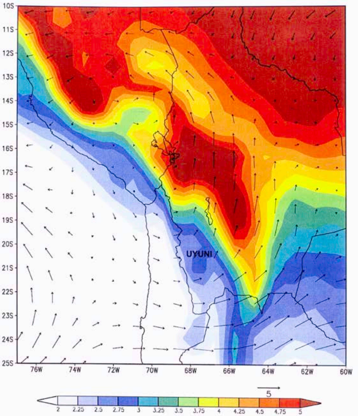

Figure 45. Horizontal wind (vectors) and mixing ratio (shaded) fields at 550 mb during LESD's constructed using the NCEP global tropospheric analyses. The winds are expressed in ms^{-1} and the mixing ratio in $g\ kg^{-1}$.

4. MESOSCALE MODELING STUDY

4.1. The numerical model

The Weather Research and Forecasting Model (WRF) is a next-generation numerical model designed for weather prediction purposes with a major focus on the simulation of mesoscale processes. It is the result of a multi-agency effort (Skamarock et al., 2005), having been developed jointly by the Mesoscale and Microscale Meteorology division of the National Center for Atmospheric Research (NCAR/MMM), the National Centers for Environmental Prediction (NOAA/NCEP), the Forecast Systems Laboratory (NOAA/FSL), the University of Oklahoma Center for Analysis and Prediction of Storms (CAPS), and the U.S. Air Force Weather Agency (AFWA).

The design of the WRF began in 1998, and it targeted the 1-10 km grid-scale for operational weather forecasting, regional climate prediction, air quality simulation, and idealized dynamical studies, with the idea of eventually replacing the existing mesoscale numerical models such as MM5, ETA and RUC. The characteristics of the WRF Model version 2.0 are described in Skamarock et al. (2005). The equations used are fully compressible Euler nonhydrostatic with a run-time hydrostatic option. The prognostic variables are the zonal and meridional components of the wind in Cartesian coordinates, vertical velocity, perturbation potential temperature, perturbation geopotential and perturbation surface pressure of dry air. The initial design allowed for multiple dynamical cores, with a dynamical core based on height coordinates and a mass core based on mass coordinates. The model uses the Arakawa-C grid for horizontal staggering and sigma coordinates in the vertical. A major advantage of the WRF over other models is the improvement of the numerical options. Large time steps utilize a third order Runge-Kutta scheme, and second to sixth order advection operators can be chosen to solve the advection equation.

4.2. Experimental design and settings

The modeling study concentrated on the Lake Titicaca region with the purpose of describing the structure of the circulations and storms that develop during the night. Fine (1.3 km) horizontal resolution simulations were made over Lake Titicaca but not over the Salar de Uyuni given the absence of clouds and precipitation over the salar. And although the study by Rife et al. (2002) for the Great Salt Lake in Utah provides information about certain surface parameters, their values are not necessary similar to those of Salar de Uyuni.

The main component of the modeling study is based on ten 24-hour long experiments carried out using the NCEP Tropospheric Global Analyses as initial and boundary conditions. These are summarized in Table 2. The 10 cases correspond to LESD's that occurred in January and early February 2003. From these experiments 6 simulations produced significant (> 10 mm day^{-1}) rainfall rates over Lake Titicaca (WET), whereas 4 produced little or no rainfall (DRY). The simulations were analyzed and compared to (1) describe the lake-induced circulations, rainfall, and thermodynamic structure associated with nocturnal convective storms, and (2) explore which factors present in the DRY and not in the WET simulations suppress the development of the nocturnal storms. Since the major goal was to describe the nocturnal processes, the simulations were initialized at 12 UTC (07 LST) to provide the model with sufficient time to reproduce the diurnal circulations and the transition into the nocturnal regime.

The simulations were carried out on a Dual-Core Intel Xeon Processor computer. A box with 150x160x31 grid points centered over Lake Titicaca was established as the simulation domain (Figure 44). The horizontal resolution considered was 1.3 km, and although not ideal for convective scale simulations, sufficient to explicitly reproduce the lake-induced convective storms. The initial and boundary conditions were extracted from the NCEP Global tropospheric analyses described in section 2.4. for the 10 days indicated in Table 2. The bottom boundary conditions used were the standard data sets available for the WRF Model. Lake Titicaca's surface temperature, originally set to 0°C in the WRF model initial temperature grid, was modified to a fixed climatological annual mean value of 13°C (Carmouze, 1991). The dynamic options chosen included the use of 3rd order Runge-Kutta schemes for the finite differencing calculations and 5th order horizontal advection and 3rd order vertical advection schemes.

The model physical options employed have also been described in Skamarock et al. (2005). Except for the microphysics and convection, most of the physical options considered follow the WRF standard configuration. Given the scale of the finer-resolution simulations the convective parameterizations were turned off, therefore the convection was resolved explicitly. The microphysical scheme (Lin et al. 1983; Rutledge and Hobbs, 1984) includes six classes of hydrometeors: water vapor, cloud water, rainwater, cloud ice, snow and graupel. This is a relatively sophisticated scheme in WRF and was chosen because ice microphysics may be important in the altiplano convective processes, given the altitudes where the convection occurs.

The land surface model used in the WRF simulations was the Noah LSM (Skamarock et al, 2005), which has the purpose of providing sensible and latent fluxes to the boundary layer scheme. Based on the MM5 OSU land surface model, the Noah LSM uses a 4-layer soil temperature and moisture model with canopy moisture and snow cover prediction included. The surface layer processes are treated with the Monin-Obukhov similarity theory using stability functions from Paulson (1970), Dyer and Hicks (1970) and Webb (1970) to compute surface exchange coefficients for heat, moisture and momentum. Four stability regimes following Zhang and Anthes (1982) and no thermal roughness length parameterization further describe the scheme. The Yonsei University (YSU) boundary layer scheme, the next generation of the MRF boundary layer scheme, was selected. It uses counter-gradient terms to represent fluxes due to non-local gradients, which adds an explicit treatment of the entrainment layer at the PBL top, and the vertical mixing is determined by the vertical stability. The RRTM longwave radiation parameterization by Mlawer et al. (1997) was employed. It is a one-dimensional (vertical) spectral band scheme that uses pre-set tables to accurately represent longwave processes due to water vapor, ozone, CO_2, and trace gases (if present), as well as accounting for cloud optical depth. For short-wave radiation the Dudhia (1989) scheme, extracted from MM5, was utilized. It is based on a simple downward integration of solar flux, accounting for clear-air scattering, water vapor absorption (Lacis and Hansen, 1974), and cloud albedo and absorption. It uses look-up tables for clouds from Stephens (1978).

Case	Run Code	Real convection	Model convection
January 26	R0	Yes	Yes
January 11	R1	Yes	No
January 22	R2	Yes	Yes
January 30	R3	Yes	No
February 01	R4	Yes	No
January 05	R5	No	No
January 18	R6	Yes	Yes
January 20	R7	Yes	Yes
January 25	R8	Yes	Yes
January 12	R9	Yes	Yes

Table 2. List of the simulations completed during the short modeling study. The first column indicates the dates extracted from the NCEP Global Tropospheric Analyses datasets as initial and boundary conditions, the second column the run code, the third indicates if convection was present in the observations, and the fourth if convection was present on the model simulations.

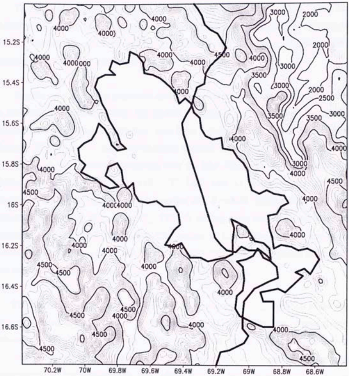

Figure 46. 160x150 –gridpoint domain used for the lake effect storm simulations carried out as part of the modeling study. The terrain elevation is plotted in units of mASL. The dark contours indicate terrain elevation every 500 m. The thin solid lines indicate terrain elevations above 3500 mASL, with contours every 50 m. The thin dashed lines indicate terrain elevations below 3500 mASL, with contoursevery 50 m. Lake Titicaca and the Peruvian-Bolivian border are indicated with a solid black line.

4.3. Simulated diurnal circulations and rainfall

This section describes mesoscale circulations and rainfall modulated by Lake Titicaca based on the results from numerical simulations with the WRF model. The characteristics of the nocturnal convective storms are explored and described, together with the atmospheric conditions associated with their development.

To gain insight into the mesoscale circulations and other meteorological fields during a nocturnal convective episode, this section discusses a particular event that produced rainfall rates larger than 20 mm day^{-1} over Lake Titicaca. The particular event is that of January 25-26, when a moist environment coupled with weak mid-tropospheric flow favored the development of convection over the lake. Figure 45 organizes six different fields averaged over the night (19 – 07 LST, last 12 hours of the simulation): accumulated rainfall (a), 630 mb divergence (b), 2 mAGL mixing ratio (c), upward sensible heat flux at the surface (d), 550 mb mixing ratio (e) and wind magnitudes averaged over the 620-570 mb layer. The surface of Lake Titicaca is located near the 640mb pressure level. The 10 mAGL wind vectors are plotted over panels (a-d), the 550 mb winds over panel (e) and the 620-570 winds over panel (f).

The simulation of the January 25-6 case shows that the average location of the region of convergence, organized into ~ 10 km wide lines (Figure 47b), was almost along the lake-axis in the south and west of the axis to the north. Although the low-level convergence appeared to be larger in the northwest sector, the largest rainfall rates were encountered in the southeastern end, which suggests that the near-surface and mid-tropospheric moisture variability may be playing a more important role in the low-level convergence variability and the intensity of the nocturnal storms. Low level-convergence showed largest values in the order of ~ 400 10^{-6} s^{-1}, low-level moisture larger than 8 g kg^{-1}, and 550 mb moisture larger than 5 g kg^{-1}. The magnitude of the upward sensible heat flux showed maximum values on the order of 50 W m^{-2}. Offshore breezes were clearly observed in the simulations starting near the edges of the lake, where the sensible

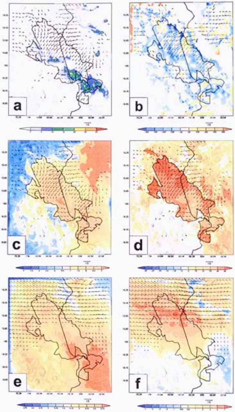

Figure 47. (a) Total rainfall in mm, (b) 630 mb divergence in 10^6 s^{-1}, (c) 2 mAGL mixing ratio in g kg^{-1}, (d) sensible heat flux at ground level in W m^{-2}, (e) mixing ratio at 550 mb in g kg^{-1}m and (f) 620-570 mb averaged winds in m s^{-1} averaged over the night (19-07 LST, last 12 hours of the simulation) for the January 25-26 wet simulation (R0). 10 mAGL winds in m s^{-1} are included in panels a, b, c, and d. 570 mb winds in m s^{-1} are included in figures e and f. Only the winds stronger than 2 m s^{-1} are plotted.

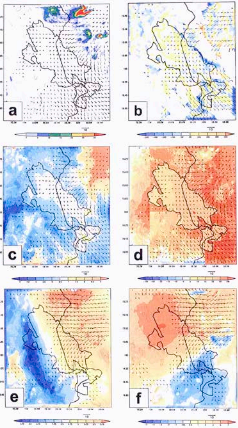

Figure 48. (a) Total rainfall in mm, (b) 630 mb divergence in 10^6 s^{-1}, (c) 2 mAGL mixing ratio in g kg^{-1}, (d) sensible heat flux at ground level in W m^{-2}, (e) mixing ratio at 550 mb in g kg^{-1}m and (f) 620-570 mb averaged winds in m s^{-1} averaged over the night (07-19 LST, first 12 hours of the simulation) for the January 25-26 wet simulation (R0). 10 mAGL winds in m s^{-1} are included in panels a, b, c, and d. 570 mb winds in m s^{-1} are included in figures e and f. Only the winds stronger than 2 m s^{-1} are plotted.

heat flux gradients were a maximum. The intensity of the breezes over the coast agreed with the observations, but was slightly stronger, with values on the order of 2-4 m s^{-1}. The winds accelerated over the lake in response to less friction (i.e. lower values of roughness length) than over land.

The daytime circulations (07 – 19 LST) were also explored and are presented in Figure 46. Less evident, but present, weak (1-2 m s^{-1}) onshore breezes can be seen in Figure 48a. The daytime breezes were weaker, in response to the weaker lake-land sensible heat flux gradient than during the night. Errors in the soil temperature initialization that diminish as the simulation progresses may be responsible for this weakenss. The effects of the 1° climatological soil temperature initialization are obvious in the sensible heat flux field (Figure 48d). Weak (< 200 10^{-6} s^{-1}) but widespread low-level divergence was observed over the lake, especially in the northern two-thirds. Although localized, the magnitude of the low-level convergence and divergence associated with the topography is larger than that associated with the lake circulations. The low-level moisture during the first part of this simulation was low, with values below 6.5 g kg^{-1} with the exception of the easternmost sector of the lake, where values slightly larger than 7 g kg^{-1} occurred. Easterly mid-tropospheric flow seemed to transport moist air from the eastern slopes into the Altiplano during the day, and veered to southeasterly towards the end of the period, transporting air from the central altiplano into the Lake Titicaca region.

The vertical structure of the atmosphere associated with the nocturnal convective events is shown in Figures 49-53. Potential temperature was first plotted (Figure 49) and used to sketch the depth of the boundary layer, whenever the atmospheric structure was sufficiently sharp to suggest it. The clearest boundary layer, as expected, was found during the day (13 LST or Figure 50a), especially over land when the depths were on the order of 600 to 800 m. The diurnal boundary layer is the shallowest over the eastern side of the lake, which was also observed in other simulations. Figure 49a illustrates this clearly for the January 25 case, when a boundary layer as shallow as ~150 m was identified. Over land, the depth of the boundary layer appears to be the largest where the sensible heat fluxes are the largest, in this case west of 70°W and east of 68.8°W (Figure 48d). After sunset the boundary layer over land disappears leading to a disguised residual layer. Over the lake, however, the boundary layer experienced a significant increase from ~150 m at 13 LST to ~500 m at 19 LST and the depth persisted during the rest of the night, starting to decrease again by 7 LST on the next day. Relative humidity and rainwater suggested the development of cloudiness over the lake by 19 LST leading to nocturnal convection by 01 LST, which persists into 07 LST. Figure 50 illustrates a cross-section of the equivalent potential temperature with distributions agreeing with the depth of the boundary layer seen from the potential temperature field. This figure illustrates the evolution of the role of the lake from a heat sink in the morning (cool and stable conditions near the surface) to a hear source during the early evening and into the night. The buoyant air generated over the lake is transported to the west by the large-scale flow leading to near-saturation humidities over a shallow layer to the west of the lake. Strong radiative cooling from the land surface creates a very stable layer underneath the high theta-e air, increasing the stability towards the early morning.

Figure 51 shows the across-lake component of the wind cross-section at 16.1°S obtained from simulation R0. Lake Titicaca is located between 69.5°W and 68.9°W. The onshore breezes are evident at 13 LST (panel a) with across-lake flow with an easterly component west of 69.4°W and with a westerly component east of this longitude. For this case the wind speeds accelerate to 1.5 m s^{-1} over the western shore and to 2 m s^{-1} near the eastern shore. As expected, the breeze circulations are contained within the boundary layer. A region of wind speeds larger than 7 m s^{-1} is evident over the eastern sector of the lake, centered at 580 mb and at 69°W. This feature is associated with the channeling effects of gap located to the east of the lake, also illustrated by figure 48. Furthermore, upslope circulations are visible over both the eastern and western mountain range with speeds that are twice those of the lake breezes. It should be pointed out that the problems in the sensible heat flux just west of the lake might be affecting these results by decreasing the wind speeds in this sector of the cross section (70 – 69.8°W), which is consistent with the simulated decrease in the boundary layer depth. A region of

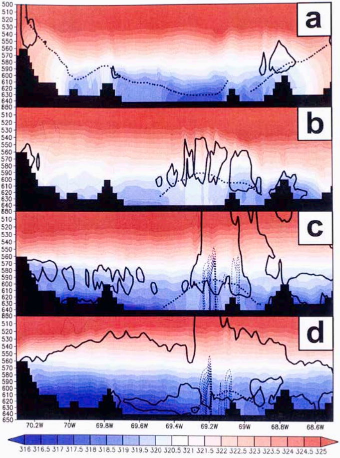

Figure 49. Cross-section at 16.1°S showing the diurnal cycle of potential temperature in °K (shaded), the 80% relative humidity contour (thin black line), the 95% relative humidity contour (thick black line) and the 5, 10, 15, 20, 25, 30, 35 and 40 10^4 g kg^{-1} rainwater contours for (a) 13 LST, (b) 19 LST, (c) 01 LST, and (d) 07 LST for the January 25-26 (R0) WET simulation. The approximate depth of the boundary layer is sketched with a dotted line.

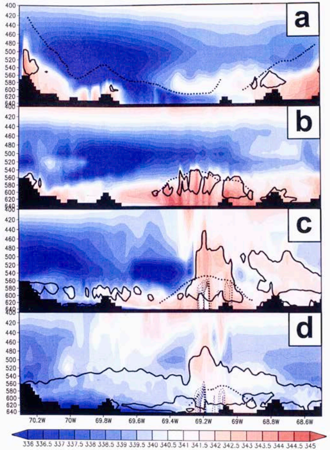

Figure 50. Cross-section at 16.1°S showing the diurnal cycle of equivalent potential temperature in °K (shaded), the 80% relative humidity contour (thin black line), the 95% relative humidity contour (thick black line) and the 5, 10, 15, 20, 25, 30, 35 and 40 10^4 g kg^{-1} rainwater contours for (a) 13 LST, (b) 19 LST, (c) 01 LST, and (d) 07 LST for the January 25-26 (R0) WET simulation. The approximate depth of the boundary layer is sketched with a dotted line following the potential temperature section displayed in figure 47.

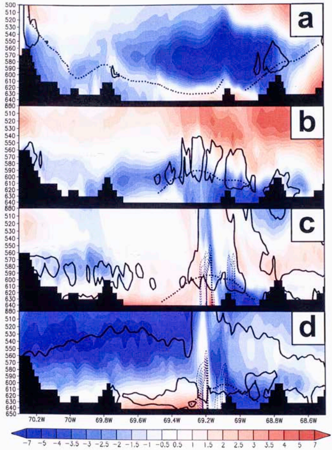

Figure 51. Cross-section at 16.1°S showing the diurnal cycle of the across-lake rotated component of the wind in m s^{-1} (shaded), the 80% relative humidity contour (thin black line), the 95% relative humidity contour (thick black line) and the 5, 10, 15, 20, 25, 30, 35 and 40 10^4 g kg^{-1} rainwater contours for (a) 13 LST, (b) 19 LST, (c) 01 LST, and (d) 07 LST for the January 25-26 (R0) WET simulation. The approximate depth of the boundary layer is sketched with a dotted line following the potential temperature section displayed in figure 47.

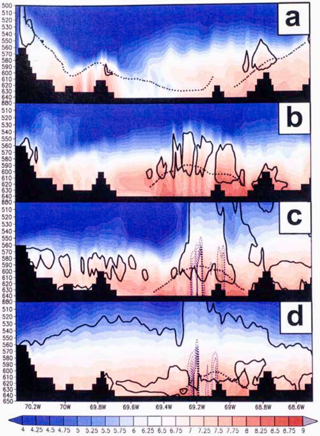

Figure 52. Cross-section at 16.1°S showing the diurnal cycle of mixing ratio in g kg^{-1} (shaded), the 80% relative humidity contour (thin black line), the 95% relative humidity contour (thick black line) and the 5, 10, 15, 20, 25, 30, 35 and 40 10^4 g kg^{-1} rainwater contours for (a) 13 LST, (b) 19 LST, (c) 01 LST, and (d) 07 LST for the January 25-26 (R0) WET simulation. The approximate depth of the boundary layer is sketched with a dotted line following the potential temperature section displayed in figure 47.

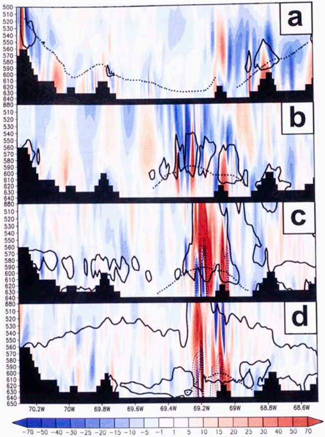

Figure 53. Cross-section at 16.1°S showing the diurnal cycle of vertical velocity in cm s^{-1} (shaded), the 80% relative humidity contour (thin black line), the 95% relative humidity contour (thick black line) and the 5, 10, 15, 20, 25, 30, 35 and 40 10^4 g kg^{-1} rainwater contours for (a) 13 LST, (b) 19 LST, (c) 01 LST, and (d) 07 LST for the January 25-26 (R0) WET simulation. The approximate depth of the boundary layer is sketched with a dotted line following the potential temperature section displayed in figure 47.

downslope winds can be found just west from the eastern mountain range located closest to the lake. The easternmost mountain range, just east of the graphed domain, is the tallest one. The complex terrain east of the lake has the largest gap in the mountain range just north of this cross section therefore its effects are only visible on the secondary mountain range.

After sunset (19 LST or panel b) the winds reverse with the region of calm winds centered in the same location (69.4°W), in the western third of the lake. The offshore breezes are also contained within the boundary layer. The flow above 550 mb becomes westerly suggesting a decay in the strength of the channeled winds as the diurnal cycle progresses. By 01 LST the offshore winds intensify to speeds greater than 3 m s^{-1} over the terrain west of the lake, shifting the region of convergence to the east, now near the center part of the lake. Smaller scale flow variations generated by the convection can be noted. By 07 LST (panel d) the breeze signal is even clearer.

The mixing ratio (Figure 52) during the simulation shows a moistening process of the altiplano boundary layer from ~ 6 g kg^{-1} over the lake at 13 LST to ~ 8 g kg^{-1} by 19 LST. The boundary layer moisture over Lake Titicaca increases from 5.5 – 7 g kg^{-1} during the day to 7.5 – 8.5 g kg^{-1} towards the evening and midnight hours. The vertical velocity field is plotted in Figure 53. It shows weak sinking motions over the lake during the day in the order of 1-10 cm s^{-1}. Updrafts associated with the storms are evident at 01 and 07 LST with speeds larger than 70 cm s^{-1}, and were a maximum at 01 LST.

4.4. Conditions that enhance and suppress nocturnal convection

The conditions that enhance and suppress nocturnal convection were explored by comparing the results from the WET and DRY simulations. Figures 54 and 55 display the simulated low-level circulations, rainfall and additional parameters similar to those presented in Figure 47 but averaged over the WET and DRY simulations. A noticeable difference in rainfall is evident from events that averaged ~10 mm^{-1} day in the WET simulations to near zero in the DRY case. A difference in the low-level wind speeds is noticeable with larger speeds during the DRY events and some of the regions of convergence displaced towards the terrain located to the southwest of the lake. During the WET simulations the winds were weaker and the region of the largest convergence aligned and just west of the lake axis. This area coincided with the region of the largest rainfall with values as high 7 mm day^{-1} that resulted from averaging the 24-hour rainfall over 6 simulations.

Low-level moisture (Figures 54c-55c) seems to be larger (~ 0.5 to 2 g kg^{-1}) over land during the WET events than during the dry ones. Over the lake, however, the values seem to fluctuate around 8 g kg^{-1} during both events. This suggests the role of the lake as a moisture source since the mixing ratio over the surface remains almost constant independent of region-wide variations in low-level moisture. This, together with the sensible heat flux field (Figures 54d-55d), which appears similar in both cases, suggests that the increase in the low-level wind speed may be related to synoptic forcing instead of surface-induced circulations. This agrees with a strong (~ 5-7 m s^{-1}) northeasterly flow at between 620 and 550 mb (Figures 55e and 55f) in contrast to weaker southeasterly flow (~ 3-5 m s^{-1}) in the same layer during the WET events (Figures 54e and 54f). The apparent mechanism for the suppression of the storms by the across-lake flow is by maintaining the region of convergence west of the lake, where the air is less buoyant during the night. The "northeasterly flow-suppression of convection" mechanism described above, consistent with the composite analysis findings, seems counterintuitive when considering that the altiplano moisture source is located to the east, however, the numerical simulations revealed that the air that enters the altiplano through the gaps located to the east of Lake Titicaca seems to be less moist during NLESD's that during LESD's. Although the effects of synoptic scale circulation anomalies such as cyclonic/rising and anticyclonic/sinking motions were discussed in section 3.3, smaller scale processes such as the moistening of the mid-troposphere by nocturnal convection immediately east of the altiplano have not been described yet. Satellite composite analyses discussed in section 3.3 and presented in Figures 37 and 42 show positive cold cloud anomalies over the eastern slopes just east of the Lake Titicaca region during the onset and development of an LESD in contrast to negative anomalies during NLESD's.

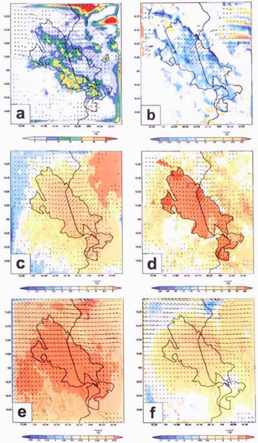

Figure 54. (a) Total rainfall in mm, (b) 630 mb divergence in 10^6 s^{-1}, (c) 2 mAGL mixing ratio in g kg^{-1}, (d) sensible heat flux at ground level in W m^{-2}, (e) mixing ratio at 550 mb in g kg^{-1}m and (f) 620-570 mb averaged winds in m s^{-1} averaged over the night (19-07 LST, last 12 hours of the simulation) averaged over the WET simulations (B0, B2, B6, B7, B8 and B9). 10 mAGL winds in m s^{-1} are included in panels a, b, c, and d. 570 mb winds in m s^{-1} are included in figures e and f. Only the winds stronger than 2 m s^{-1} are plotted.

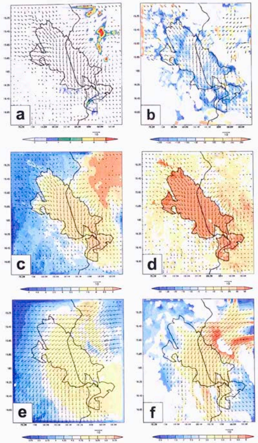

Figure 55. (a) Total rainfall in mm, (b) 630 mb divergence in 10^6 s^{-1}, (c) 2 mAGL mixing ratio in g kg^{-1}, (d) sensible heat flux at ground level in W m^{-2}, (e) mixing ratio at 550 mb in g kg^{-1}m and (f) 620-570 mb averaged winds in m s^{-1} averaged over the night (19-07 LST, last 12 hours of the simulation) averaged over the DRY simulations (B1, B3, B4 and B5). 10 mAGL winds in m s^{-1} are included in panels a, b, c, and d. 570 mb winds in m s^{-1} are included in figures e and f. Only the winds stronger than 2 m s^{-1} are plotted.

They support the hypothesis stated above, suggesting that an environment favorable for the development and maintenance of nocturnal convection over Lake Titicaca is favored by the advection of moister air produced by convection to the east of the lake.

The most evident difference between the two cases is the moisture content at 550 mb. Whereas DRY events are characterized by domain-wide mixing ratios that vary between 4 and 5 g kg^{-1}, during WET events the mixing ratios larger than 5.5 g kg^{-1}. The atmospheric differences on the equivalent potential temperature field (Figures 56 and 57) suggest that the major difference between the two classifications is the moisture content, since the temperatures were slightly cooler during the WET simulation. Largest moisture differences appear to occur around 600-500 mb layer, which is the region of the atmosphere located near or immediately over the nocturnal Lake Titicaca boundary layer. This further suggests that dry air entrainment from mid-tropospheric air into the boundary layer could be the major storm suppressor, which requires more study. From the simulations it appears that nocturnal convection develops and maintains when the moisture immediately above the boundary has mixing ratios larger than 7 g kg^{-1}, contrasting with suppressed convection when the ratios are in below 7 g kg^{-1}. This difference can be associated with mid-tropospheric air (i.e. air above the nocturnal altiplano boundary layer) homogeneous equivalent potential temperature values in the order of 342°K versus a vertical gradient from 341°K in the upper boundary layer to 339°K at ~ 520 mb respectively.

Figures 58 and 59 indicate that DRY periods are associated with slightly weaker breeze signal when compared to the WET ones. Together with these findings, the vertical motions, analyzed and displayed in Figures 60 and 61 illustrate that the magnitude of the updrafts seems to be larger during WET and DRY events. During the day, the structure of the sinking motions seems to be similar for both cases, but the regime changes to rising motions over the lake faster in the WET simulations. Furthermore, wider regions of rising motion occur during the wet events., and the main difference that the atmosphere is far from saturation (Figures 60c and 61c).

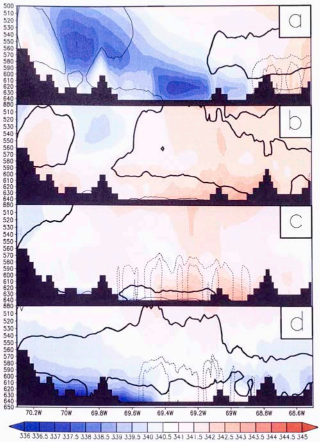

Figure 56. Cross-section at 16.1°S showing the diurnal cycle of equivalent potential temperature in °K (shaded), the 80% relative humidity contour (thin black line), the 95% relative humidity contour (thick black line) and the 5, 10, 15, 20, 25, 30, 35 and 40 10^4 g kg^{-1} rainwater contours for (a) 11-15 LST, (b) 17-21 LST, (c) 23-03 LST, and (d) 05-07 LST averaged over the WET simulations (B0, B2, B6, B7, B8 and B9).

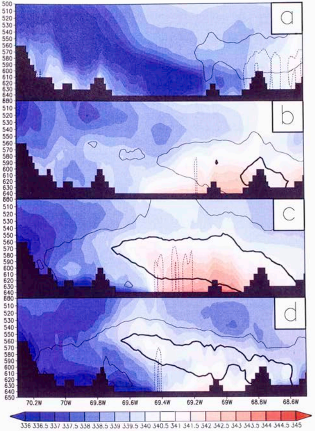

Figure 57. Cross-section at 16.1°S showing the diurnal cycle of equivalent potential temperature in °K (shaded), the 80% relative humidity contour (thin black line), the 95% relative humidity contour (thick black line) and the 5, 10, 15, 20, 25, 30, 35 and 40 10^4 g kg^{-1} rainwater contours for (a) 11-15 LST, (b) 17-21 LST, (c) 23-03 LST, and (d) 05-07 LST averaged over the DRY simulations (B1, B3, B4 and B5).

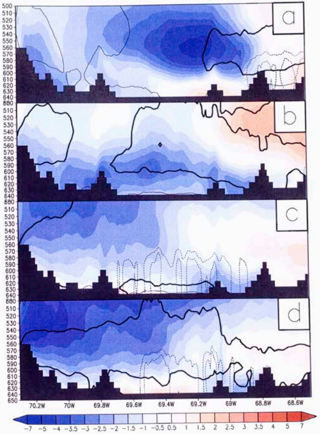

Figure 58. Cross-section at 16.1°S showing the diurnal cycle of the across-lake rotated component of the wind in m s^{-1} (shaded), the 80% relative humidity contour (thin black line), the 95% relative humidity contour (thick black line) and the 5, 10, 15, 20, 25, 30, 35 and 40 10^4 g kg^{-1} rainwater contours for (a) 11-15 LST, (b) 17-21 LST, (c) 23-03 LST, and (d) 05-07 LST averaged over the WET simulations (B0, B2, B6, B7, B8 and B9).

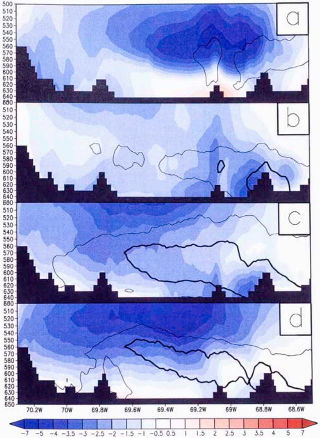

Figure 59. Cross-section at 16.1°S showing the diurnal cycle of the across-lake rotated component of the wind in m s^{-1} (shaded), the 80% relative humidity contour (thin black line), the 95% relative humidity contour (thick black line) and the 5, 10, 15, 20, 25, 30, 35 and 40 10^4 g kg^{-1} rainwater contours for (a) 11-15 LST, (b) 17-21 LST, (c) 23-03 LST, and (d) 05-07 LST averaged over the DRY simulations (B1, B3, B4 and B5).

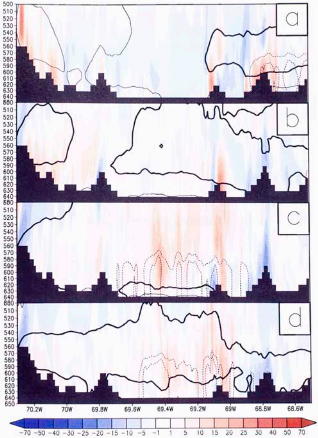

Figure 60. Cross-section at 16.1°S showing the diurnal cycle of vertical velocity in cm s^{-1} (shaded), the 80% relative humidity contour (thin black line), the 95% relative humidity contour (thick black line) and the 5, 10, 15, 20, 25, 30, 35 and 40 10^4 g kg^{-1} rainwater contours for (a) 11-15 LST, (b) 17-21 LST, (c) 23-03 LST, and (d) 05-07 LST averaged over the WET simulations (B0, B2, B6, B7, B8 and B9).

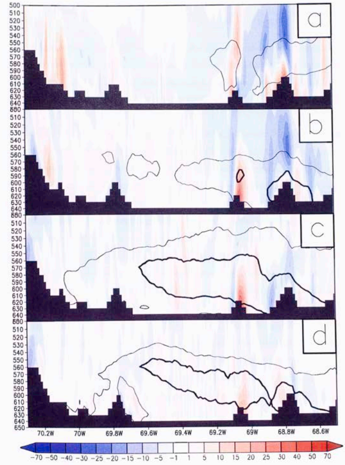

Figure 61. Cross-section at 16.1°S showing the diurnal cycle of vertical velocity in cm s^{-1} (shaded), the 80% relative humidity contour (thin black line), the 95% relative humidity contour (thick black line) and the 5, 10, 15, 20, 25, 30, 35 and 40 10^4 g kg^{-1} rainwater contours for (a) 11-15 LST, (b) 17-21 LST, (c) 23-03 LST, and (d) 05-07 LST averaged over the DRY simulations (B1, B3, B4 and B5).

5. SUMMARY AND CONCLUSIONS

The mesoscale circulations induced by Lake Titicaca and Salar de Uyuni along with the associated rainfall, were described using daily rainfall observations, wind data from pilot balloons, satellite infrared data, numerical model analyses and numerical model simulations carried out with the Weather Research and Forecasting (WRF) model.

Analysis of the rainfall data showed that the largest rainfall rates in the northern Altiplano occur over Lake Titicaca associated with nocturnal convective storms, which although shallower and less frequent than the afternoon convection, produce larger rainfall rates with totals that exceed 200 mm month^{-1} over the lake and almost twice the ~ 110 mm month^{-1} observed over land. Both the lake and the salar induce weak onshore and offshore winds of similar magnitudes (1-2 m s^{-1} for the Lake and 1-3 m s^{-1} for the Salar) and depths (700-1400 mASL) that start during the morning (09 LST) and extend into the mid-afternoon (15 LST). Low-level divergence associated to this pattern of circulation is present over both features with larger values and more prolonged periods over the salar (40-110 x 10^{-6} s^{-1}) than over the lake (10-60 x 10^{-6} s^{-1}). Offshore winds induced by the lake between 05 and 08 LST with magnitudes of 1-2 m s^{-1} produce low-level convergence in the 0 to –60 x 10^{-6} s^{-1} range. Over the salar, however, offshore winds are not evident during this time of the day and the flow remains slightly divergent. The arrival of flow originating on the eastern (western) slopes of the Andes into the altiplano covers Lake Titicaca (Salar de Uyuni) with sustained winds that exceed 15 m s^{-1} and leads to strong low-level convergence on the order of –40 to –100 x 10^{-6} s^{-1} (-40 to -250 x 10^{-6} s^{-1}). The latter produces strong convection over the lake but none over the salar, which suggests that additional factors are necessary for the development and maintenance of the convective storms.

The altiplano circulations were further described using the WRF model. The simulations produced breezes of similar speeds but slightly shallower depths (~ 700-1000 mAGL). The diurnal breezes were underestimated given lower diurnal sensible heat fluxes over land due to problems with the initialization of the soil temperature. The depth of the boundary layer was evident from these simulations, which indicated very shallow (~15 mb deep) diurnal boundary layers over the lake. During the night, in contrast, deeper boundary layers develop over the lake associated to the convergence of the low-level breezes. These reach their maximum depth (~ 60 mb) around 01 LST.

The simulations also suggested that the lake acts as a nocturnal heat and moisture source revealed by weak variations in the sensible heat flux and in the near-surface mixing ratio, even when the moisture over the land surrounding the lake varies. Large low level mixing ratios on the order of 8 g kg^{-1} were common over the lake during the night. Induced vertical velocities in response to the low-level convergence are, according to the simulations, on the order of ~0.7 m s^{-1}. These generate convection with cloud tops that fluctuate around -15°C depending on the strength of the convective event.

Numerical simulations suggested that the intensity and location of the nocturnal storms is regulated by the synoptic circulation, which controls the availability of low-level moisture over the altiplano and, the strength and orientation of the mid-tropospheric flow, and therefore the location of the regions of maximum convergence. The essential factor for convection to be sustained appears to be a moist environment in the layer immediately over the altiplano nocturnal boundary layer, which is ~ 550 mb. Widespread high moisture values larger than 5.5 g kg^{-1} and a homogeneous layer of equivalent potential temperature of 342°K were present at this level during the days in which the convection developed and persisted. This further suggests that dry air entrainment into the top of the boundary layer is the main factor that suppresses the maintenance of the nocturnal convective storms, when the low-level environment is favorable for their formation.

Additional results from the observational study and the numerical model simulations suggested that nocturnal convective events are associated with southeasterly anomalies of the flow over the altiplano, which favor the transport of moisture from the lowlands in southern Bolivia into the region. This type of circulation pattern, together with low-wind/high-moisture conditions over the northern altiplano favor the development of the nocturnal storms, since the orientation of the large scale flow, aligned with the lake axis, preserves the position of the low-level convergence over the lake. In contrast, northeasterly mid-tropospheric flow, channeled by the gap in the topography to the northeast of Lake Titicaca, suppresses the convective development by maintaining the region of low-level convergence away from the heat and moisture source.

To conclude, the factors necessary for the development and maintenance of nocturnal convective storms in the altiplano are (1) moist low-level convergence induced by a local source of heat and moisture such as Lake Titicaca, (2) large moisture contents near and below the 550 mb layer, and (3) mid-tropospheric flow sufficiently weak to maintain the region of low-level convergence over the heat and moisture source. These factors, periodically present over the lake region during the rainy season, do not occur over the salar. Changes in the salar surface properties coupled with changes in the large-scale circulation pattern may be necessary for nocturnal convective storms to develop over it.

REFERENCES

Abbott, M. B., B. B. Wolfe, A. P. Wolfe, G. O. Seltzer, R. Aravena, B. G. Mark, P. J. Polissar, D. T. Rodbell, H. D. Rowe, M. Vuille, 2003: Holocene paleohydrology and glacial history of the central Andes using multiproxy lake sediment studies. *Palaeogeography, Palaeoclimatology, Palaeoecology*: Vol. 194, pp. 123-138.

Aceituno, P., 1997: Climate elements of the South American Altiplano. *Rev. Geofis.*, Vol. 44, pp. 37-55.

Aceituno, P., and A. Montecinos, 1993: Circulation anomalies associated with dry and wet periods in the South American Altiplano. Preprints, *Fourth Int. Conf on Southern Hemisphere Meteorology*, Hobart, Australia, Amer. Meteor. Soc., pp. 37-55.

Baker, P. A., G. O. Seltzer, S. C. Fritz, R. B. Dunbar, M. J. Grove, P. M. Tapia, S. L. Cross, H. D. Rowe, J. P. Broda, 2001: The History of South American Tropical Precipitation for the Past 25000 Years. *Science*, Vol. 291, pp. 640-643.

Baker, P. A., C. A. Rigsby, G. O. Seltzer, S. C. Fritz, R. B. T. K. Lowenstein, N.P. Bacher, C. Veliz, 2001: Tropical climate changes at millennial timescales on the Bolivian Altiplano. *Nature*, Vol. 409, pp. 698-701.

Blodgett, T. A., J. D. Lenters and B. L. Isacks, 1997: Constraints on the Origin of Paleolake Expansions in the Central Andes. *Earth Interactions*, Vol. 1, N°1, pp. 1-28.

Bourges, J., J. Cortes and E. Salas, 1992: Hydrological Potential. In "Lake Titicaca a synthesis of limnological knowledge" (C. Dejoux and A. Iltis, eds), pp. 523-538. Kluwer Academic Publishers, Dordrecht, Boston, London.

Carmouze, J.P., 1991: El Balance Energético, El Lago Titicaca, *ORSTROM pub*, pp. 149-160.

Constantini, M. L., L. Sabetta, G. Mancinelli and L. Rossi, 2003: Spatial variability of the decomposition rate of Schnoenoplectus tatora in a polluted area of Lake Titicaca. *Journal of Tropical Ecology*. Volume 20, 1-11.

Douglas, M. W., and W. Fernandez, 1997: Strengthening the meteorological sounding network over the tropical eastern Pacific ocean and the intertropical Americas. *World Meteorological Organization WMO*. Volume 46, N°4, 348-351.

Davies-Jones, R., 1993: Useful formulas for computing divergence, vorticity and their errors from three or more stations, *Monthly Weather Review*, Vol. 121, pp. 713-725.

Dudhia, J., 1989: Numerical study of convection observed during the winter monsoon experiment using a mesoscale two-dimensional model, *J. Atmos. Sci*, Vol. 46, 3077-3107.

Dyer, A.J. , B.B. Hicks and V. Sitaraman. 1970: Minimizing the Levelling Error in Reynolds Stress Measurement by Filtering. *Journal of Applied Meteorology*: Vol. 9, No. 3, pp. 532–534.

Endlich, R. M. and J.R. Clark. 1963: Objective Computation of Some Meteorological Quantities. *Journal of Applied Meteorology*: Vol. 2, No. 1, pp. 66–81.

Garreaud, R. D., and P. Aceituno, 2000: Intraseasonal Variability of Moisture and Rainfall over the South American Altiplano. *Monthly Weather Review*: Vol. 128, No. 9, pp. 3337–3346.

Garreaud, R. D., 1999: Multiscale Analysis of the Summertime Precipitation over the Central Andes. *Monthly Weather Review*: Vol. 127, No. 5, pp. 901–921.

Gellert, W., H. Küstner, M., Hellwich, and H. Kästner, Eds., 1977: The VNR Concise Encyclopedia of Mathematics. Van Nostrad Reinhold, 760 pp.

Instituto Geográfico Militar, 1997: Atlas de Bolivia, Bolivia, 272 pp.

Jellison, R, Y. S. Zadereev, P. A. DasSarma, J. M. Melack, M. R. Rosen, A. G. Degermendzhy, S. DasSarma, and G. Zambrana, 2004: Conservation and Management Challenges of Saline Lakes: A Review of Five Experience Briefs.

Kessler, A., 1984: The paleohydrology of the Late Pleisctocene Lake Tauca on the southern Altiplano (Bolivia) and recent climatic fluctuations. *SASQUA INTERNATIONAL SYMPOSIUM*, Swaziland, pp. 115-122.

Kreizig, E., 1988: Advanced Engineering Mathematics, 6th ed. Wiley and Sons, 1413 pp.

Lacis, A. A., and J. E. Hansen, 1974: A parameterization for the absorption of solar radiation in the earth's atmosphere. *J. Atmos. Sci*, Vol. 31, 118-133.

Lenters, J. D., and K. H. Cook, 1999: Summertime precipitation variability over South America: The role of the large-scale circulation, *Mon. Wea. Rev.*, 127, 409-431.

Lin, Y., R. D. Farley and H. D. Orville. 1983: Bulk Parameterization of the Snow Field in a Cloud Model. *Journal of Applied Meteorology*: Vol. 22, No. 6, pp. 1065–1092.

Mlawer, E. J., S. J. Taubman, P. D. Brown, M. J. Iacono, and S. A. Clough, 1997: Radiative transfer for inhomogeneous atmosphere: RTTM, a validated correlated-k model for the long-wave. *J. Geophys. Res.*, Vol. 102 (D14), pp. 16663–16682.

Parrish, D. F. and John C. Derber. 1992: The National Meteorological Center's Spectral Statistical-Interpolation Analysis System. *Monthly Weather Review*: Vol. 120, No. 8, pp. 1747–1763.

Paulson, C. A., 1970: The Mathematical Representation of Wind Speed and Temperature Profiles in the Unstable Atmospheric Surface Layer. *Journal of Applied Meteorology*: Vol. 9, No. 6, pp. 857–861.

Pedder, M. A. 1981: On the Errors of Kinematic Vertical Motion Estimation Using Divergence Bias Adjustment Procedures. *Monthly Weather Review*: Vol. 109, No. 8, pp. 1813–1816.

Peña, M, 1999: Characteristics of Central American Wet and Dry Spells. M.S. Thesis, Department of Meteorology, University of Oklahoma, 97 pp.

Placzek, C., J. Quade, and J. P. Patchett, 2004: Lake History of the Southern Bolivian Altiplano (18-22°S) over the last 120 KA. Denver Anual Meeting (November 7-10, 2004).

Revollo, M, M. Liberman, and A. Lescano, 2003: Lake Titicaca. In "Lake Basin Management Initiative – Regional Workshop for Europe, Central Asia and the Americas", Vermont, USA.

Rife, D., T. Warner, F. Chen and E. Astling, 2002: Mechanisms for diurnal boundary layer circulations in the Great Basin Desert, *Monthly Weather Review*, Vol 130, pp. 921-938.

Ronteltap M., J. Rieckermann, and H. Daebel, 2004: Managements Efforts at Lake Titicaca. The Science and Politics of International Freshwater Management. Swiss Federal Institute of Technology Zurich.

Rutledge, S. A. and P. V. Hobbs. 1984: The Mesoscale and Microscale Structure and Organization of Clouds and Precipitation in Midlatitude Cyclones. XII: A Diagnostic Modeling Study of Precipitation Development in Narrow Cold-Frontal Rainbands. *Journal of the Atmospheric Sciences*: Vol. 41, No. 20, pp. 2949–2972.

Schwerdtfeger, W., 1976: Climates of Central and South America. *World Survey of Climatology*. Volume 12, 532 pp.

Skamarock, W.C., J. B. Klemp, J. Dudhia, D. O. Gill, D. M. Barber, W. Wang, and J. G. Powers, 2005: A description of the Advanced Research WRF Versión 2. *NCAR technical note*. 88 pp.

Stephens, G. L., 1978: Radiation profiles in extended water clouds. Part II: Parameterization schemes. *J. Atmos. Sci.*, Vol. 35, 2123-2132.

Sylvestre, F., S. Servant-Vildary, and M. Roux 2001: Diatom-based ionic concentration and salinity models from the south Bolivian Altiplano (15-23°S). *Journal of Paleolimnology*. Volume 25, 279-295 pp.

Trauth, M. H., B. Bookhagen, N. Marwan, and M. R. Strecker, 2003: Multiple landslide clusters record Quaternary climate changes in the northwestern Argentine Andes. *Palaeogeography, Palaeoclimatology, Palaeoecology*: Vol. 194, pp. 109-121.

Vuille, M., 1999: Atmospheric circulation over the Bolivian Altiplano during DRY and WET periods and extreme phases of the Southern Oscillation. *Int. J. Climatol.*, 19, 1579-1600.

Vuille, M., D. R. Hardy, C. Braun, F. Keimig, and R. S. Bradley, 1998: Atmospheric circulation anolamies associated with 1996/97 summer precipitation events on Sajama ice cap, Bolivia. *J. Geophys. Res,* 103, Vol. 11, pp. 191-204.

Vuille, M., and C. Ammann, 1997: Regional snowfall patterns in th high, arid Andes. *Climatic Change*: Vol. 36, pp. 413-423.

Webb, E. K., 1970: Profile relationships: The log-linear range, and extension to strong stability, *Quart. J. Roy Meteor*. Soc, Vol. 96, pp. 67-90.

Weinreb, M. P., Jonson, J. X., and D. Han: 2001: Conversión of GVAR Infrared Data to Scene Radiance or Temperature. NOAA NESDIS Office of Satellite Operations. Available through internet (http://www.oso.noaa.gov/goes/goes-calibration/gvar-conversion.htm).

Zhang, D.-L., and R. A. Anthes, 1982: A high-resolution model of the planetary boundary layer-sensitivity tests and comparisons with SESAME-79 data. *J. Appl. Meteor.*, Vol. 21, pp. 1594-1609.